ELECTROMAGNETICALLY COUPLED MICROSTRIP PATCH ANTENNAS - THEORETICAL AND EXPERIMENTAL INVESTIGATIONS

A Thesis

Submitted to

the College of Graduate Studies and Research

in Partial Fulfillment of the Requirements for

the Degree of

Master of Science

in the

Department of Electrical Engineering

The University of Saskatchewan

By

NEMAI CHANDRA KARMAKAR

Saskatoon, Saskatchewan

December, 1991

☆☆☆☆☆☆☆☆☆☆☆☆☆

DEDICATED TO
THE MEMORY OF MY FATHER

☆☆☆☆☆☆☆☆☆☆☆☆☆

COPYRIGHT

ACKNOWLEDGMENT

During the course of the work done on this thesis I have received generous support from a number of people. In particular, I wish to thank my supervisor (external) Dr. A. K. Bhattacharyya for his enthusiastic support of my project. To my supervisor Dr. R.J. Bolton, and to Dr. S.O. Kasap, I am thankful for their patience in putting up with the proof reading of my thesis and invaluable suggestions.

The bulk of work of my research was done at the Center for Communication Research of the Department of Electrical Engineering, University of Saskatchewan. For this opportunity, I thank Prof. S. Kumar, the Head of the center, and Mr. G. Wells for his technical assistance in using the HP8510B Network Analyzer.

Financial assistance provided by the Natural Science and Engineering Research Council of Canada is thankfully acknowledged, as is thanks to Dr. M. S. Sachdev, Prof. and Head of the department of Electrical Engineering, for taking care of the financial support for the last couple of months.

Finally, I owe a special thank you to my wife Shipra Karmakar, for her understanding and for giving the opportunity to do this work.

UNIVERSSITY OF SASKATCHEWAN
Electrical Engineering Abstract 92A356

ELECTROMAGNETICALLY COUPLED MICROSTRIP PATCH ANTENNAS - THEORETICAL AND EXPERIMENTAL INVESTIGATIONS

Student: N.C. Karmakar Supervisor: Dr. R.J. Bolton

Supervisor: Dr. A.K. Bhattacharyya (External)

December 1991

ABSTRACT

In recent years microstrip patch radiators have been playing an increasing role in antenna design. The light weight, low profile and conformability of microstrip antennas make them very attractive for aircraft, missile and satellite applications.

One of the promising method of feeding energy to the radiating element that was suggested recently is to couple the feedline electromagnetically to the patch radiator. This novel feed mechanism has the advantages of effective coupling, ease of fabrication, reduced spurious radiation from the feed network and large bandwidth. This method provides for flexibility in choosing the substrates which best meet the conflicting requirement of dissimilar substrates for feed network and patch radiator.

In this thesis, an improved model is proposed for accurate evaluation of an electromagnetically coupled (EMC) rectangular patch antenna. In the proposed model, the antenna is viewed as a planar waveguide which is excited by a magnetic surface current.

The equivalent circuit for the feed line and waveguide transition is developed. Effects of the stored energy and radiated energy are incorporated in the equivalent circuit.

Numerical results for the input impedance and the return loss of the EMC patch antenna are obtained from the proposed model and from the two other existing models. The results were compared with the measured data (experiments were conducted in the Electrical Engineering laboratory). The proposed model is found to have a better agreement than the existing models with respect to the return loss and the input impedance of an EMC microstrip antenna.

TABLE OF CONTENTS

LIST OF SYMBOLS

$\vec{A}$	magnetic vector potential
a	length of the patch
b	width of the patch
B_r	radiation susceptance
c	feed inset under the patch
C^+, C^-	incident and reflected mode field amplitude coefficients
cos	cosine function
d	thickness of the lower substrate
e	exponential operator
E_{mn}	mn-th mode amplitude coefficient for electric field
E_{zp}	z-directed primary feed line electric field
$\vec{E}$	electric field
f	frequency
F_{mn}	mn-th mode amplitude coefficient for vector electric potential
$\vec{F}$	vector electric potential
G_r	radiation conductance
h	thickness of the upper substrate

$\vec{H}$	magnetic field
$\vec{J}$	electric surface current density
k	propagation constant
k_0	propagation constant in free space
L	length of the feed line
ln	natural logarithm
$\vec{M}$	magnetic surface current
n	turns ratio of ideal transformer
$\hat{n}$	unit normal over a surface
$\vec{P}$	Poynting vector
P_r	radiation power
P_s	stored power in the patch cavity
P_t	total power
r	distance of the observation point from the origin
R_r	radiation resistance
RL	return loss
sin	sine function
tan	tangent function
V_0	voltage across the radiation slots
V_{op}	primary feed voltage

V_s	secondary patch voltage
V^+, V^-	voltages at x=0 and x=c respectively
w	width of the feed line
r	distance of the observation point from the origin
X_r	radiation reactance
Y_{in}	input admittance of the antenna
Y_r	radiation admittance
Z_f	characteristic impedance of the feed line
Z_{in}	input impedance of the antenna
Z_L	load impedance
Z_o	characteristic impedance of the patch
Z_r	radiation impedance
x,y,z	rectangular coordinate systems
Δl	extended length of the truncated patch
β	propagation constant
β_f	propagation constant of the feed line
$\delta(x)$	Dirac-Delta function of x
∇	Delta operator
ε	permittivity
ε_d	dielectric constant of the lower substrate
ε_{eff}	effective dielectric constant of the substrate

ε_h	dielectric constant of the upper substrate
ε_0	permittivity of vacuum
ε_r	relative dielectric constant of the substrate
λ_0	free space wavelength
μ	permeability
r,θ,ϕ	spherical coordinate system
η	intrinsic wave impedance
ψ_m	scalar magnetic potential
ω	angular frequency
π	3.1415.....
$\hat{}$	unit vector notation
$\rightarrow$	vector notation

LIST OF FIGURES

1. INTRODUCTION

1.1 General

In recent years microstrip radiators have been playing an increasing role in antenna design. The light weight, low profile and conformability of microstrip antennas make them very attractive for aircraft, missile, rocket and satellite applications. The other usages of microstrip antennas are in biomedical radiators, Doppler or other portable radars, radio altimeters, environmental instrumentation, remote sensing, etc. [1].

There are many different varieties of microstrip antennas [2], but their common feature is that they basically consist of four parts:

a) a very thin flat metallic region often called the patch;

b) a dielectric substrate;

c) a ground plane which is usually much larger than the patch; and

d) a feed which supplies the patch element with radio frequency power.

In its simplest form, a microstrip antenna is composed of a radiating microstrip patch connected to the feed line and separated from the ground plane by a dielectric as shown in figure-1.1.

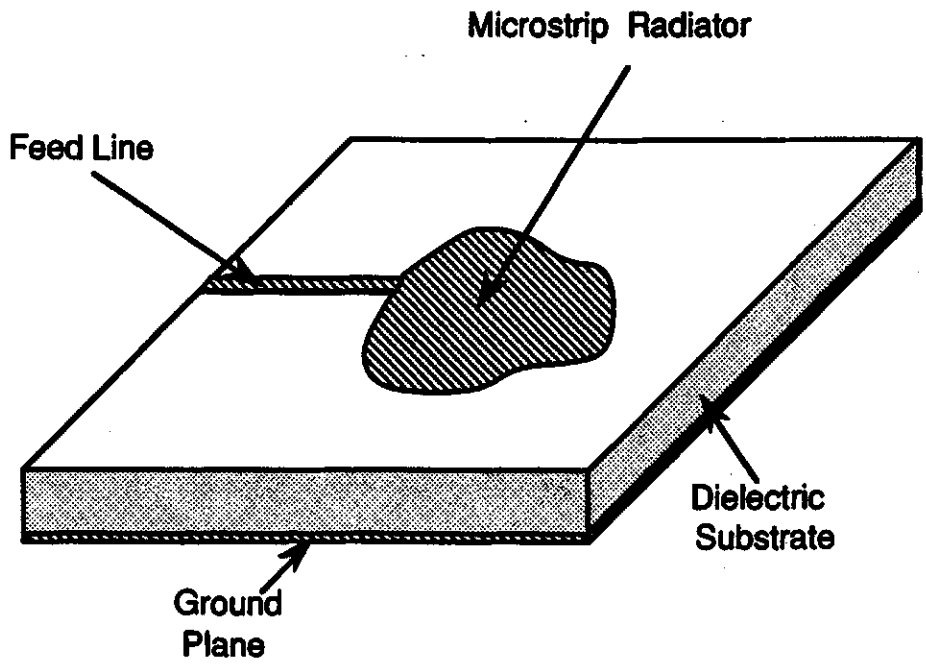

Figure-1.1 A microstrip patch antenna;

As illustrated in figure-1.1, the radiating patch and the feed line are etched on the upper surface of the dielectric with a ground plane on the lower surface. The antenna is excited by the feed line. The patch and feed conductors are normally of copper or gold. The patch element can be of any shape but the choice is made so that the analysis of the radiation mechanism is simplified. Typical shapes of the patches are rectangles, circles and rings. Ideally, the dielectric constant of the substrate should be low ($\varepsilon_r \sim 2.5$) so as to enhance the fringe fields which account for the radiation [1].

The excitation (feeding) of the patch antennas presents both practical and analytical difficulties. In monolithic microwave integrated circuit (MMIC), the radiating element and the feed circuitry are fabricated on the

same semiconductor substrate [3,4]. Materials with high dielectric constants are required for feed circuit. The patch elements are etched on the materials with low dielectric constants for efficient radiation. This conflicting requirement leads the antenna designer to examine for the efficient feed mechanism. There are various types of feed mechanisms for microstrip patch antennas. The feed mechanisms can be classified into three broad categories [5]:

a) direct contact feeds,

b) electromagnetically coupled or proximity feeds,

c) aperture coupled feeds.

a) Direct Contact feed

Direct contact feeds are the most common form of coupling. A direct feed is realized by using a microstrip transmission line etched upon the same dielectric substrate. The line is connected to the patch at its edge. Two examples of edge connected fed microstrip antennas are shown in figure 1.2(a). Another form of direct contact feed is the coaxial probe feed shown in figure 1.2(b). A coaxial feed is obtained by running the coaxial line to a suitable point on the ground plane and connecting the inner conductor through the substrate to the radiator and the outer conductor is connected to the ground plane. In both cases, impedance matching is accomplished by varying the location of the feed-patch connection point.

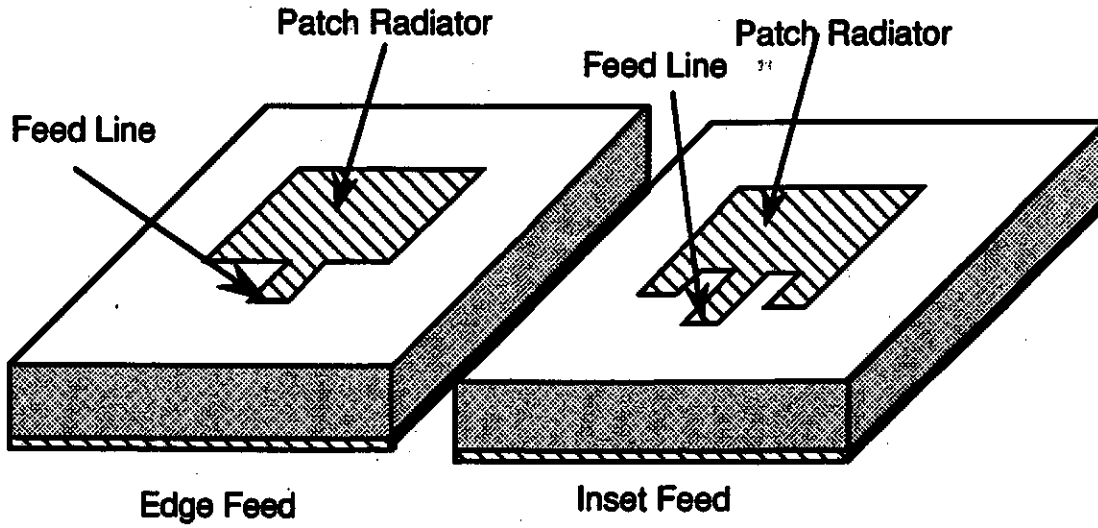

(a) Microstrip Line Feeds

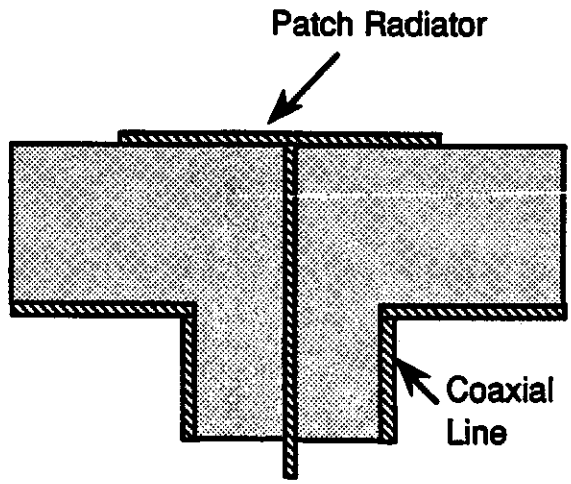

(b) Inset Coaxial Feed

Figure-1.2 Direct contact feeds;

A problem with direct contact feeds is that the patch has a high-radiation impedance located at the edge; obtaining a good match to a practically useable size of transmission line feed may be difficult and requires an intensive matching network [6]. This can be avoided if the feed voltage is applied at a point within the resonant field structure of the patch

which is at a lower voltage than that at the edge. An impedance transformation effect then occurs and good matching to any desired impedance may gradually be obtained.

b) Electromagnetically coupled or proximity feeds

Electromagnetically coupled or proximity feeds can provide this impedance transformation effect. Proximity fed patches are electromagnetically coupled by being in close proximity to the feed line. The patch and the feed line can be either on the same surface or vertically separated. Modification of direct contact feeds provides two examples of proximity coupled feeds as shown in figure 1.3(a) and 1.3(b). In the case of direct connection of microstrip feed line if a gap exists between the patch and the feed, the patch is coupled electromagnetically to the feed with the gap spacing controlling the amount of power coupled. This type of coupling is called *capacitive coupling* [6].

Variation on the ideas may be made by using a multilayer dielectric with the feed line closer to the ground plane than the radiator. The feed is coupled to the patch by the fringe fields through the upper substrate as shown in figure 1.3(b). The substrates may be of different materials or may be of the same material. This arrangement has the advantage of the reducing unwanted feed radiation which may be a problem with single-layer substrates. There is also the possibility of saving space by placing a part of the feed network underneath the patch radiator provided the coupling problem can be overcome. Patch bandwidth can also be increased by using a thicker upper dielectric substrate material and also by adjusting the feed configuration under the patch [7]. Choice of different dielectric

substrates for the patch elements and the feed lines offers an added advantage [8].

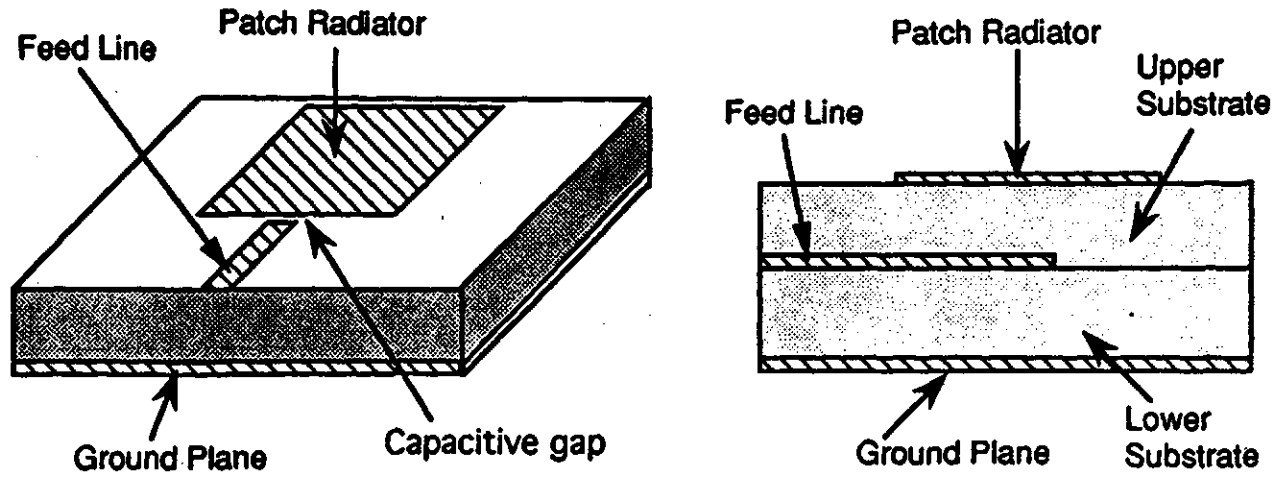

(a) Palanar feed with capacitive gap

(b) Double layer EMC feed

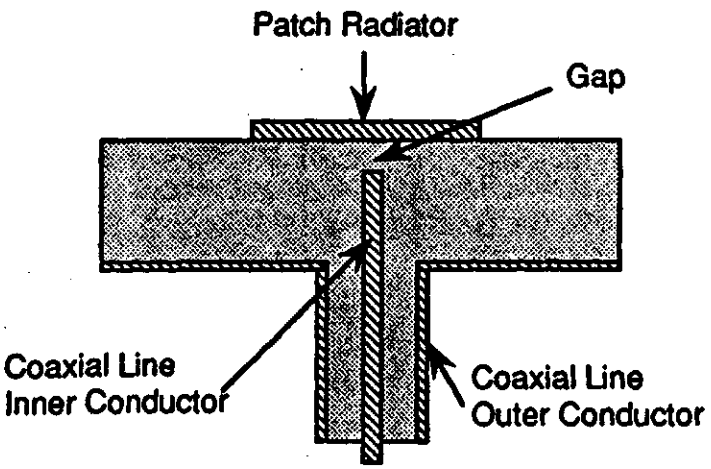

(c) EMC coaxial probe feed

Figure-1.3 Proximity feed configuration

In the case of coaxial probe modification, the probe feed does not have to connect with the patch in order to couple energy to it, as shown in figure 1.3(c).

c) Aperture coupled feeds

Aperture coupling provides a method which also allows the use of different substrates for the patch and the active circuitry [9,10]. The feed circuitry is placed on the bottom of the lower substrate. The substrates are separated by a ground plane which has an aperture cut into it to allow coupling electromagnetically to the patch which is on the upper substrate.

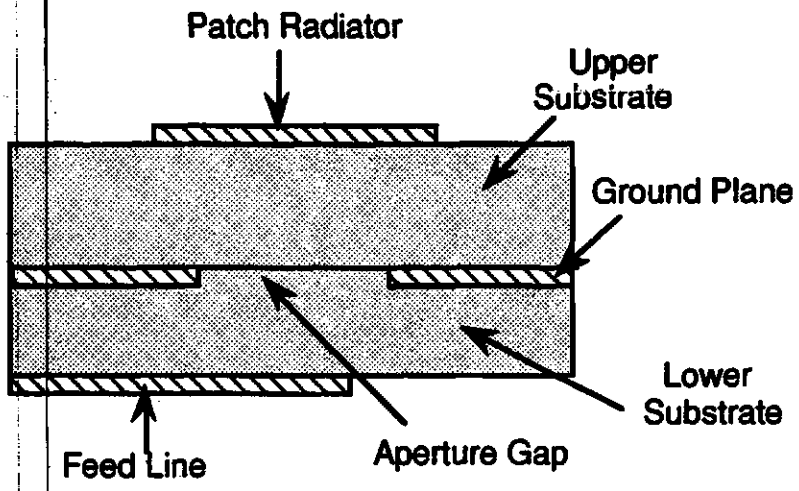

Figure-1.4 An aperture coupled antenna element

The increased constructional complexity of the antenna is a problem for this type of antenna. Shown in figure-1.4 is an example of an aperture coupled microstrip antenna element.

1.2 Electromagnetically Coupled Microstrip Patch Antenna

The double layer proximity fed antenna shown in figure-1.3(b) is called electromagnetically coupled (EMC) microstrip patch antenna in the nomenclature. This type of antenna has many advantages over the direct contact feds and the aperture coupled elements. The positive features of EMC microstrip patch antennas are as follows:

1) spurious radiation due to the discontinuity from the feed network can be reduced by decreasing the height and increasing the dielectric constant of the lower substrate;

2) patch bandwidth can be increased by using a thicker upper substrate;

3) good impedance matching and maximum power transfer are possible by varying the feed inset under the patch and by using different dielectric layers with different thicknesses;

4) it can be made conformal like other microstrip antennas;

5) higher gain is possible by varying the feed and patch dimension;

6) it is simple in construction since patch antenna and feed network can be fabricated separately; and

7) the EMC patch antenna arrays are possible to design.

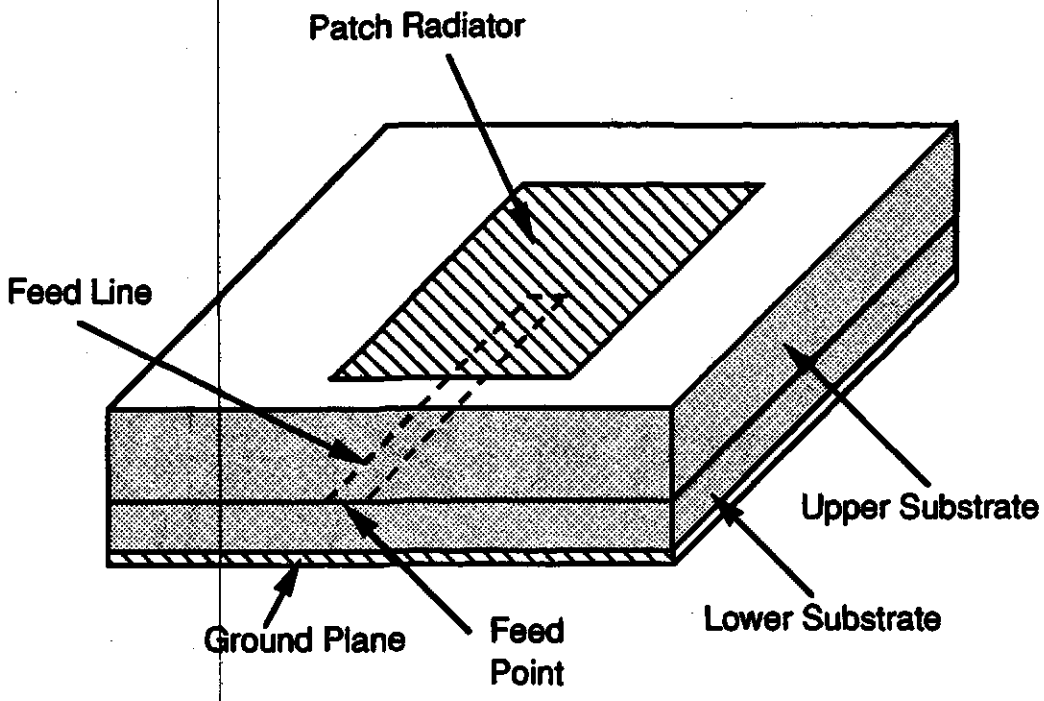

Figure-1.5 An electromagnetically coupled rectangular microstrip patch antenna

The geometry of an EMC rectangular microstrip patch antenna is shown in figure-1.5. The structure is composed of two-layer substrates. In general substrates are of different thicknesses and permittivity. The lower substrate is made thinner than the upper substrate, so that feed line radiation pattern will be less disturbed [11]. The upper substrate is made thicker and has a low dielectric constant for high efficiency and large bandwidth [12,13]. However, both the substrates can be made of same dielectric material with the same thickness. The microstrip feed line is printed on the lower substrate with the bottom surface as the ground plane. The microstrip patch is printed on the upper substrate bonded to the feed structure. The feed line is centered with respect to the patch width, and is

inset a distance from the edge of the patch. The feed inset is sometimes termed 'overlap' in the literature [14].

1.3 Thesis Objectives

Due to its inherent simplicity in construction and better performance, the EMC microstrip patch antenna has recently, therefore, gained the attention of antenna researchers. To obtain a simplified design formula, it is, therefore, worthwhile to undertake the study of an EMC patch antenna. The use of different types of substrates with different thicknesses and embedded planar feed circuitry, gives the designer some added flexibility.

In order to design a practical array antenna using electromagnetic coupling [15], it is essential that the characteristics of a single element be understood. The objectives of this thesis are to investigate theoretically and experimentally the electromagnetic coupling of a rectangular microstrip patch antenna element for the general practical case of dissimilar substrates in a 3.5 to 4.5 Ghz frequency range. The theoretical and practical investigations will culminate in the production of design curves which will allow the designer to determine the best antenna dimensions for a given input impedance, as well as resonant frequency. In order to accomplish this, the input impedance over a range of frequencies for different feed-patch dimensions (patch dimensions with feed inset as a parameter) must be determined.

In order to calculate the input impedance of an EMC microstrip patch antenna element different approaches are considered. In each approach, a generalized transmission line model (except the cavity modal method) is developed. By using the circuit model, the input impedance of the patch radiator seen by the feed line is determined. The electromagnetic coupling of the feed line and the patch radiator via dielectric substrates is represented by an ideal transformer. Knowing the input impedance of the patch and the turns ratio of the transformer, the total input impedance of an EMC microstrip patch antenna can be obtained. Once the input impedance of the antenna is obtained, different characteristic parameters such as resonant resistance, resonant frequency, return loss, and bandwidth can be determined.

The theory which follows allows one to determine the patch dimensions and feed inset required to obtain a good match. With this estimate it is then possible to design experimental samples. The measured data can be used to verify the theoretical developments. Proposed analytical method undertaken in this thesis is simpler than the avaliable method.

The specific objectives for the present research work are as follows:

1) Analytical investigations of the characteristics of the EMC microstrip patch antennas.

2) Development of an appropriate analytical technique that can be used to predict the performances of an EMC microstrip patch antenna accurately.

3) Validification and comparison of different approaches undertaken in this thesis with respect to the performance of different rectangular patches using the same feed network.

4) Development of design procedures for the EMC microstrip patch antenna structure under consideration.

1.4 Thesis Outlines

In this chapter different feed mechanisms of the microstrip patch antennas, and the geometry of an EMC microstrip patch antenna are presented. The thesis objectives have been outlined.

Three different methods used for the analysis of an EMC microstrip patch antenna are : (1) Transmission line model, (2) Modal expansion or cavity modal analysis, and (3) Planar waveguide model.

In Chapter-2 characteristics of an EMC microstrip patch antenna utilizing the transmission line model is analyzed. In this model the patch element is viewed as a very wide microstrip transmission line. Two slots at both ends of the line represent the radiation loss. The feed-patch transition is represented by an ideal transformer connected in series with the line. Combining the effects of the radiation loss and the feed-patch transition a circuit model is developed. From the circuit model the input impedance of an EMC microstrip patch antenna is derived.

The modal expansion or the cavity modal analysis for the EMC microstrip patch antenna is presented in Chapter-3. The source of the antenna excitation is assumed to be a magnetic surface current at the tip of the feed line. The eigenfunction associated with each mode is derived as a

function of the antenna dimensions. The power radiated and the energy stored into the cavity are formulated with the derived fields. Due to the small height of the antenna structure only TM_{10} mode is considered in the derivation. The input impedance is derived from the total complex power of the cavity.

In Chapter-4 the planar waveguide model of an EMC microstrip patch antenna is proposed. The patch antenna is assumed to be an infinitely long planar waveguide in both directions. The source is assumed to be a magnetic surface current source confined inside the planar waveguide. The reciprocity theorem is invoked to determine the unknown electric field excited by the source. By using the field solution the equivalent circuit of the source is developed. The radiation effect of the patch antenna is incorporated by two radiation impedances terminated at both ends of the equivalent circuit. The feed-patch transition is represented by an ideal transformer and related circuitry. The input impedance of the EMC microstrip patch antenna is then readily obtained from the circuit model.

Chapter-5 begins with a comparison of the results determined from the experimental data and those obtained from the theoretical analyses undertaken in this thesis. Thus the validity of the theoretical methods has been checked. The comparison is also used to predict the performance characteristics of the EMC patch antenna in terms of return loss, resonant input resistance, the resonant frequency and bandwidth. Finally, theoretical design curves are produced using the results obtained from the planar waveguide model.

Chapter-6 contains the summary and conclusions.

2. TRANSMISSION LINE MODEL

2.1 Introduction

In the preceding chapter the different analytical methods used in this thesis were briefly introduced. This chapter presents the analysis of an electromagnetically coupled (EMC) rectangular microstrip patch antenna utilizing the transmission line model. The method views the rectangular microstrip patch antenna as a wide microstrip transmission line [2,16] propagating TEM modes. The length of the line is equal to the length of the patch. The characteristic impedance of such a wide transmission line is usually low and equal to the characteristic impedance of the patch element. The radiation takes place due to the sudden discontinuity of the current lines on the patch and hence from the two ends of the patch [17]. The region between the patch edges and the ground plane at the two ends of the line can be viewed as radiating apertures much like slot antennas. Thus the low impedance line can be thought of as being loaded at its two ends not by open circuits but by high impedance loads. The load impedance is called the *radiation impedance* of the aperture. There is also a mutual coupling between the slots. To keep mathematics simple, the mutual coupling is not considered in the analysis.

The feed line supplies the radio frequency input power. The fringe electric fields at the truncated end of the feed line excites the patch radiator. The feed-patch transition is represented by an ideal transformer in the circuit model of an EMC patch antenna. The formulation of the input impedance of the antenna is derived from the circuit model. The other

characteristic parameters such as resonant frequency, bandwidth, input resistance at resonance, return loss can be found from the input impedance data.

2.2 Formulation

The geometry of an EMC microstrip patch antenna is shown in figure-2.1. The structure consists of two different dielectric substrate layers stacked one over the other. The relative dielectric constants of the upper and lower layers are ε_h and ε_d, and the thicknesses are h and d respectively. The truncated microstrip feed line is located at the interface of the two dielectric substrate layers. The width of the feed line is w, the length is L of which c is the feed inset under the patch radiator. The length of the patch antenna is a and the width is b. The feed line is centered with respect to the patch width. The voltage between the feed line edge and the ground plane is V_{op} and the voltage between the patch edge and the ground plane is V_{os}. The former one is the *cause*, which excites the patch radiator, called the primary feed line voltage, and the later one is the *effect*, induced by the former one, called secondary patch voltage as shown in figure 2.1(b). Since the primary source voltage and the secondary induced voltage have, in general, different values, the transition between the feed line and the patch radiator can be viewed as an ideal transformer in the circuit model of the EMC patch antenna. The turns ratio of the transformer will be found from the ratio of the two voltages.

As mentioned earlier, the radiation from the patch radiator takes place at both ends of the microstrip patch much like slot antennas. The radiation effect of the patch is incorporated into the equivalent transmission line of the patch by two load impedances (radiation impedances) at both

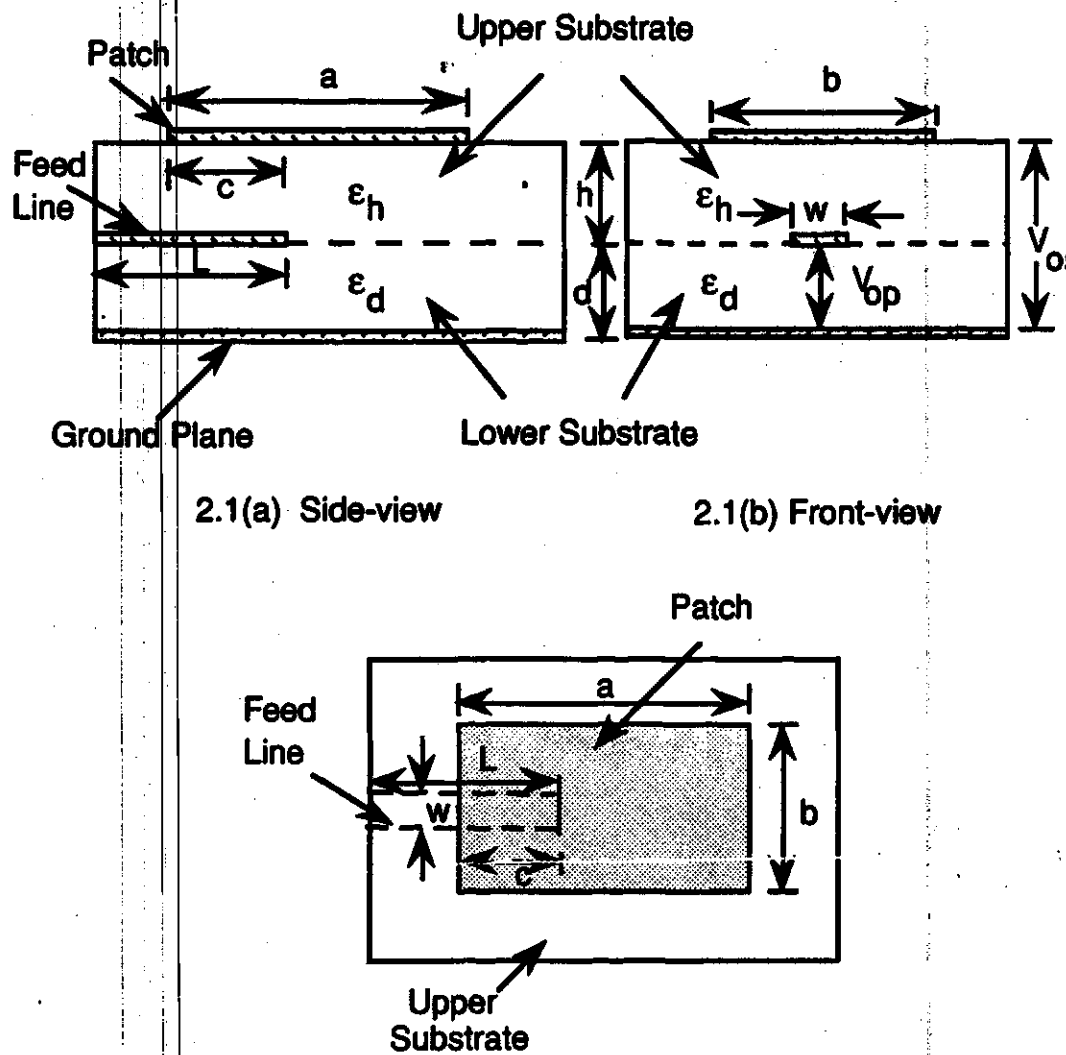

Figure-2.1 Geometry of an electromagnetically coupled microstrip antenna

ends of the line. The real part of the impedance is called the radiation resistance or input resistance of the antenna, that represents the real power loss by radiation from the slots, and thus related to the radiated far-fields. The imaginary part of the impedance is called the radiation reactance of the antenna. This represents the reactive energy stored in the

radiating slots, and is thus related to the non-propagating near-fields [18]. To understand the radiation mechanism of the patch radiator, the expressions for the radiation resistance and the radiation reactance are needed. In the following section the formulation for the radiation resistance will be derived by using the electric vector potential method [19].

2.2.1 Radiation Resistance

The microstrip radiator element may be treated as a line resonator with no transverse field variations [1]. The fields in the cavity vary along the length, which is usually a half-wavelength ($\lambda/2$) long, and radiation occurs mainly from the fringe electric fields at the open-circuited ends. The radiator may be represented as two slots spaced a distance a apart as shown in figure 2.2(a). The slot width is considered to be (d+h), equal to the substrate thickness and its length is equal to b, the width of the radiating patch as shown in fig.2.2(b). Thus the radiating slots, each has an area of b×(d+h). The electric field on the slot surface is considered to be the secondary source of radiation. Each slot radiates the same fields as a magnetic dipole and using the equivalence principle, the magnetic surface current at the aperture is given by

$$\vec{M} = 2\vec{E}_x \times \hat{n} = 2E_x \hat{x} \times \hat{y} = 2E_x \hat{z} = 2\frac{V_o}{d+h}\hat{z}\,, \quad |z| \le b/2 \qquad (2.1)$$

where, $\hat{n}$ is the unit normal on the radiating slots and in the present case $\hat{n} = \hat{y}$. The factor 2 arises due to the positive image of $\vec{M}$ over the ground plane, and V_o is the effective voltage across the center of the slot which is invariant with z-axis over its width.

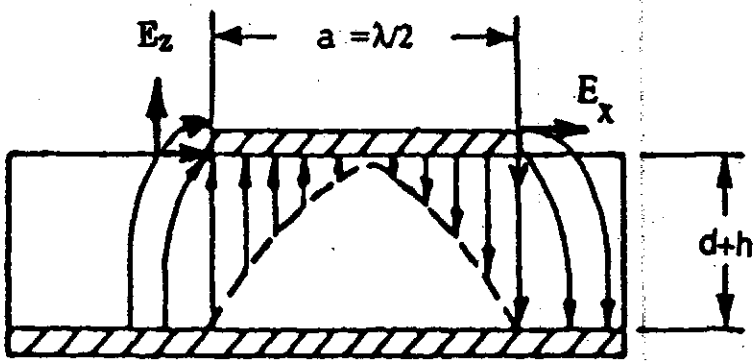

Fig.2.2(a) Fringe electic field at patch edges

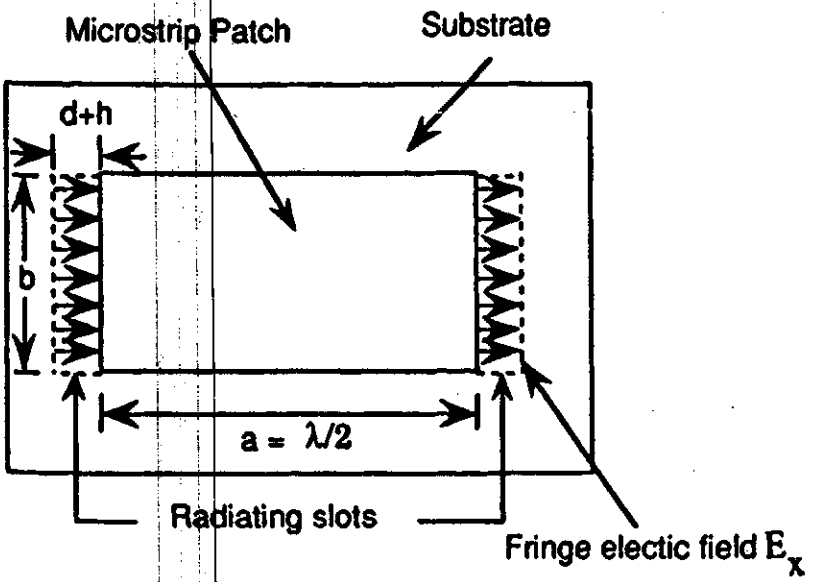

Fig. 2.2(b) Patch with two radiatiog slots

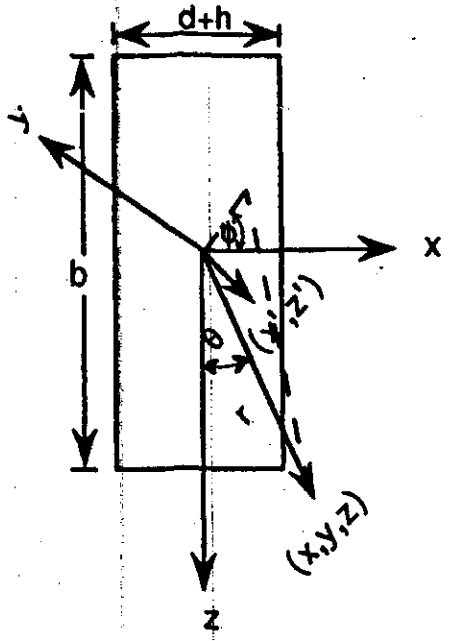

Fig.2.2(c) Radiating slot geometry (Refer to left slot of Fig.2.2(b)

Figure-2.2 Microstrip antenna with (a) fringe electric field at patch edges, (b) two radiating slots, (c) the slot geometry and coordinates

The radiation field at a distance r from the origin may be calculated by using the electric vector potential method. An electric vector potential function generated by the source distribution (2.1) is found by integrating over the source (radiation slot) point and can be written as [20]

$$F_z = 2V_o b \frac{e^{-jk_o r}}{4\pi r} \frac{\sin(\frac{k_o(d+h)}{2}\sin\theta\cos\phi)}{\frac{k_o(d+h)}{2}\sin\theta\cos\phi} \frac{\sin(\frac{k_o b}{2}\cos\theta)}{\frac{k_o b}{2}\cos\theta}, \qquad (2.2)$$

where, k_o is the propagation constant in free space and is given by $k_o = \frac{2\pi}{\lambda_o}$.

The radiation electric field at a distance r from the origin is obtained from (2.2). The far field approximation will only give a ϕ-directed component of the radiated electric field

$$E_\phi = j\, 2k_o V_o b \frac{e^{-jk_o r}}{4\pi r} \frac{\sin(\frac{k_o(d+h)}{2}\sin\theta\cos\phi)}{\frac{k_o(d+h)}{2}\sin\theta\cos\phi} \frac{\sin(\frac{k_o b}{2}\cos\theta)}{\frac{k_o b}{2}\cos\theta} \sin\theta. \qquad (2.3)$$

Considering the substrate thickness (d+h) is very small (a small fraction of a wavelength), $k_o \frac{d+h}{2} << 1$, the pattern expression becomes

$$E_\phi = jV_o \frac{e^{-jk_o r}}{\pi r} \frac{\sin(\frac{k_o b}{2}\cos\theta)}{\cos\theta} \sin\theta\,. \qquad (2.4)$$

To determine the total radiation power from the slot the magnitude of the Poynting vector needs to integrate over a hemisphere of large radius. Since the slot radiates only on one side the total power radiated from the slot is then obtained by integrating (2.4) over half the hemisphere on the slot plane [20]

$$P_r = \int_{\phi=0}^{\pi/2} \int_{\theta=0}^{\pi} \frac{|E_\phi|^2}{\eta} r^2 \sin\theta \, d\theta \, d\phi, \qquad (2.5)$$

where, η is the free space wave impedance and is given by $\eta = 120\pi\ \Omega$.

Substituting the value of E_ϕ from (2.4), the expression for P_r can be written as

$$P_r = \frac{V_o^2}{2\pi\eta} \int_{\theta=0}^{\pi} \frac{\sin^2(\frac{k_o b}{2}\cos\theta)}{\cos^2\theta} \sin^3\theta \, d\theta,$$

or,

$$P_r = \frac{V_o^2}{240\pi^2} I_1, \qquad (2.6)$$

where,

$$I_1 = \int_{\theta=0}^{\pi} \sin^2(\frac{k_o b}{2}\cos\theta)\tan^2\theta\sin\theta \, d\theta. \qquad (2.7)$$

Since Vo is the voltage drop across the center of the slot, a radiation conductance may be defined as the conductance, placed across the center of the slot [20], which will dissipate the same power as that radiated by the slot,

$$G_r = \frac{2P_r}{V_o^2} = \frac{I_1}{120\pi^2} = \frac{1}{R_r}. \qquad (2.8)$$

where, R_r is the radiation resistance. For $b << \lambda_0$, where, λ_0 is the free space wavelength, the integration I_1 can be approximated to give

$$G_r = \frac{b^2}{90\lambda_0^2}, \tag{2.9}$$

and the corresponding radiation resistance can be written as

$$R_r = \frac{V_0^2}{2P_r} = \frac{90\lambda_0^2}{b^2} \quad \text{for } b << \lambda_0.$$

For a large patch width ($b >> \lambda_0$), Harrington [21] estimates the radiation conductance per unit length (with the approximation $kb << 1$)

$$G_r = \frac{\pi}{\lambda_0 \eta} = \frac{1}{120\lambda_0},$$

and the radiation conductance for large patch of width b can be written as

$$G_r = \frac{b}{120\lambda_0} \text{ for } b >> \lambda_0. \tag{2.10}$$

The formulae for G_r may be replaced with good accuracy by the following three relations , depending on the value of b/λ_0 [6] :

$$G_r = \frac{b^2}{90\lambda_0^2} \quad \text{for } b < 0.35\lambda_0, \tag{2.11a}$$

$$G_r = \frac{b}{120\lambda_0} - \frac{1}{60\pi^2} \quad \text{for } 0.35\lambda_0 < b < 2\lambda_0, \tag{2.11b}$$

$$G_r = \frac{b}{120\lambda_0} \quad \text{for } b > 2\lambda_0. \tag{2.11c}$$

The above radiation conductance formula can be used as the equivalent conductance at the radiating edges of the rectangular patches with considerable accuracy.

2.2.2 Radiation Reactance

The rectangular patch is considered to be a thin cavity with magnetic walls in its periphery [20]. The tangential magnetic fields are zero along the fictitious magnetic wall. The magnetic walls are taken slightly away from the physical periphery to account for the stored energy in the fringe fields as shown in fig.2.3(a). The stored energy is equivalent to a susceptance at the slots, represented by a capacitor, due to the end effect of the patch and is given by Hammerstad [22]. He gives an approximate extension length of Δl of an open microstrip circuit

$$\Delta l = 0.421(d+h)\frac{\varepsilon_{eff} + 0.3}{\varepsilon_{eff} - 0.258}\quad \frac{\frac{b}{d+h} + 0.262}{\frac{b}{d+h} + 0.813}, \tag{2.12}$$

where, ε_{eff} is the effective permittivity of the two-layer substrates and is given by [6]

$$\varepsilon_{eff} = \frac{\varepsilon_r+1}{2} + \frac{\varepsilon_r-1}{2}\{1 + \frac{10(d+h)}{b}\}^{-1/2}. \tag{2.13}$$

ε_r is the relative dielectric constant of the two layer substrates and can be written as [21]

$$\varepsilon_r = \frac{d+h}{\frac{h}{\varepsilon_h} + \frac{d}{\varepsilon_d}} \quad \text{for } (d+h) << b. \tag{2.14}$$

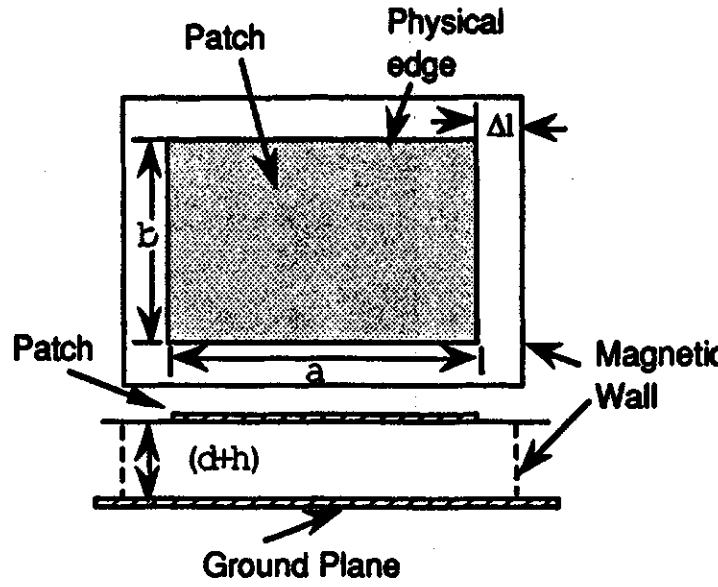

Fig.2.3(a) Patch surrounded by magnetic walls

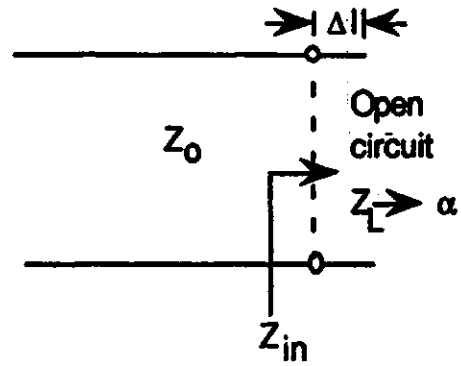

Fig.2.3(b) Transmission line equivalent of extended length Δl

Figure-2.3 Patch cavity with exterior region surrounded by magnetic wall

The equivalent susceptance which represents the energy stored in the extended length Δl , can be approximated as the input admittance of an open ended microstrip line of length Δl as shown in fig.2.3(b). The line has the characteristic impedance (Z_0) equal to that of the patch. The expression for Z_0 of a patch of width b over a substrate of thickness (d+h) is given by [6]

$$Z_0 = \frac{377}{2\sqrt{\varepsilon_r}}\left[\frac{b}{2(d+h)} + 0.441 + 0.082\frac{\varepsilon_r - 1}{\varepsilon_r} + \frac{\varepsilon_r + 1}{2\pi\varepsilon_r}\left\{1.451 + \ln\left(\frac{b}{2(d+h)} + 0.941\right)\right\}\right]^{-1/2}, \quad b/(d+h) > 1. \tag{2.15}$$

For the open circuited extended length Δl, the radiation susceptance or wall susceptance [20] can be written as

$$jB_r = j\beta\frac{\Delta l}{Z_0}, \tag{2.16}$$

where, β is the propagation constant and given by

$$\beta = \frac{2\pi}{\lambda_0}\sqrt{\varepsilon_{eff}} = k_0\sqrt{\varepsilon_{eff}}. \tag{2.17}$$

Combining (2.11) and (2.16) the radiation admittance Y_r of a patch at its open ends can be written as

$$Y_r = \frac{1}{Z_r} = G_r + j\,B_r, \tag{2.18}$$

where, the radiation impedance Z_r of the patch is the reciprocal of (2.18).

2.3 Modal Expansion of Feed Source

The primary excitation coefficient of the antenna is considered to be the fringe electric field located between the truncated end of the microstrip feed line and the ground plane. Since the distance between the feed line and the ground plane is very small (a small fraction of a wavelength), the only component of $\vec{E}$ is in the z-direction and considered to be uniform along z. Thus the z-directed primary electric field E_{zp} in terms of the primary source voltage V_{op} can be written as

$$\vec{E}_{zp} = \begin{cases} \frac{V_{op}}{d}\hat{z} & \text{for } w/2-b/2 \le y \le w/2+b/2,\ 0 \le z \le d,\ 0 \le x \le a \\ 0 & \text{otherwise} \end{cases} \qquad (2.19)$$

In the cavity model of a microstrip antenna, the patch and the substrate structure is considered to be a thin resonant cavity, a region between the patch metalization and the ground plane, surrounded by the magnetic walls around the edge of the patch [8]. Both the patch and the ground plane are assumed to be electric walls (the electric conductors). The primary electric field E_{zp} excites all the interior TE modes in the cavity. This field, using appropriate boundary conditions, can be expressed as a Fourier series expansion [21] as follows

$$E_{zp} = \sum_{mn} E_{mn} \cos(\frac{m\pi y}{b}) \cos(\frac{n\pi z}{d+h}), \qquad (2.20)$$

where, E_{mn} are the mode amplitude coefficients of z-directed electric fields mode vectors. In order to determine the coefficients E_{mn}, multiplying both sides of (2.20) by $\cos(\frac{m\pi y}{b}) \cos(\frac{n\pi z}{d+h})$ and integrating over the cross-section of the patch yields

$$\int_{y=0}^{b} \int_{z=0}^{(d+h)} E_{zp} \cos(\frac{m\pi y}{b}) \cos(\frac{n\pi z}{d+h})\, dz\, dy$$

$$= E_{mn} \int_{y=0}^{b} \int_{z=0}^{(d+h)} \cos^2(\frac{m\pi y}{b}) \cos^2(\frac{n\pi z}{d+h})\, dz\, dy. \qquad (2.21)$$

Substitution for the value of E_{zp} from (2.19) yields

$$\frac{V_{op}}{d} \int_{y=b/2-w/2}^{b/2+w/2} \int_{z=0}^{d} \cos\left(\frac{m\pi y}{b}\right) \cos\left(\frac{n\pi z}{d+h}\right) dz dy$$

$$= E_{mn} \int_{y=0}^{b} \int_{z=0}^{(d+h)} \cos^2\left(\frac{m\pi y}{w}\right) \cos^2\left(\frac{n\pi z}{d+h}\right) dz\, dy. \qquad (2.22)$$

Since the substrate is electrically thin (a small fraction of a wavelength), the dominant mode that excites in it is considered to be TE_{00} (to y) mode only. The excitation coefficient E_{00} (to y) for the dominant TE_{00} mode would be given by

$$\frac{V_{op}}{d} \times wd = E_{00}\, b(d+h), \qquad (2.23)$$

or,

$$E_{00} = V_{op} \frac{w}{b(d+h)}. \qquad (2.24)$$

The secondary voltage between the patch and the ground plane associated with the dominant mode at the location x=c is given by

$$V_{os} = E_{00} \times (d+h) = V_{op} \frac{w}{b}, \qquad (2.25)$$

or,

$$\frac{V_{os}}{V_{op}} = \frac{w}{b}. \qquad (2.26)$$

The ratio of the secondary voltage to the primary voltage represents the transition of the feed source and the patch radiator. The transition will

be viewed as an ideal transformer in the circuit model as if the power supplied by the feed to the patch is totally radiated. Thus the turns ratio of the ideal transformer representing the feed-patch transition can be written as

$$n = \frac{w}{b}. \qquad (2.27)$$

2.4 Circuit Model

The general approach for obtaining the input impedance of a microwave device is to analyze the same from a circuit point of view and develop an equivalent circuit model [23]. The same is true for a microstrip antenna. In the transmission line model of the patch element, the patch is viewed as a microstrip transmission line with radiation slots at both ends. The slots are equivalent to a load impedance (admittance) which is called the radiation impedance (admittance) of the patch antenna. The radiation impedance (admittance) formula is presented in equation (2.18). The equivalent circuit model of the patch radiator can therefore be illustrated by two radiation impedances separated by a transmission line of low impedance as shown in figure-2.4. The characteristic impedance of the line is the same as the characteristic impedance of the patch element given in equation (2.15).

The remaining task is to couple the feed line source with the existing circuit model of the patch radiator shown in figure-2.4(a). The primary source is a lateral magnetic surface current source (precisely speaking a magnetic line current source, since the spacing between the feed line and ground plane is very small) at x=c. For the lateral magnetic current source,

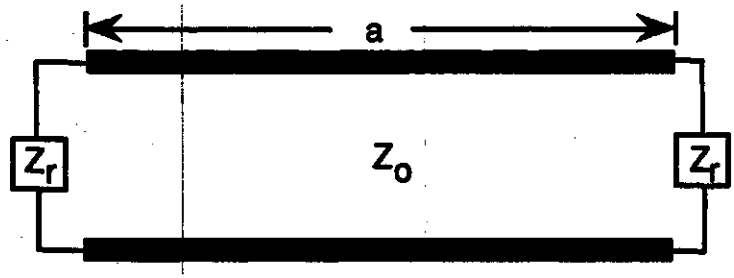

2.4(a) Equivalent circuit of a patch element

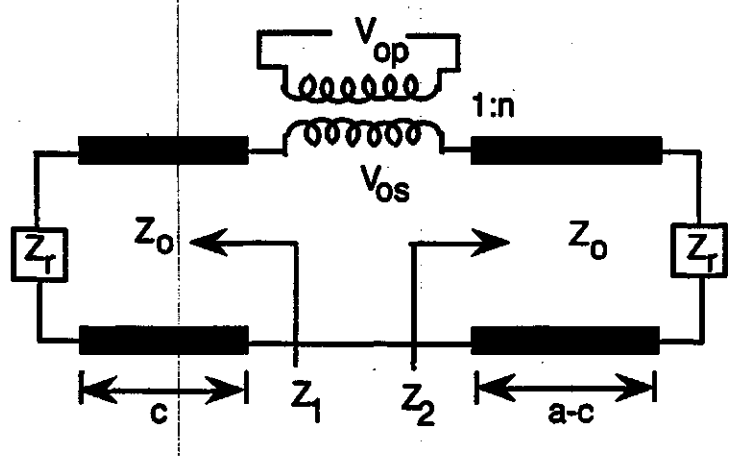

2.4(b) Equivalent circuit of an EMC patch antenna

Figure-2.4 Equivalent circuit model of an EMC patch antenna

the transverse electric fields are discontinuous $[\vec{M} = (\vec{E}_1 - \vec{E}_2) \times \hat{n}]$ across the source [24]. The source is thus equivalent to a voltage generator at x=c connected in series via an ideal transformer with the equivalent transmission line as shown in figure-2.4(b). The voltage drop of the line across the source is represented by a secondary voltage V_{os}. The primary voltage is the feed line voltage V_{op} [see figure-2.1(c)]. The ratio of the voltages is derived in the preceding section and is given in equation (2.27).

The ratio is the turns ratio (n) of the ideal transformer representing the feed-patch transition.

The impedances Z_1 and Z_2 in the circuit model in figure 2.4(b), are the input impedances of the transmission line sections of length c and (a-c) respectively where,

$$Z_1 = Z_0 \frac{Z_r + jZ_0\tan(\beta c)}{Z_0 + jZ_r\tan(\beta c)}, \qquad (2.28)$$

and,

$$Z_2 = Z_0 \frac{Z_r + jZ_0\tan\{\beta(a-c)\}}{Z_0 + jZ_r\tan\{\beta(a-c)\}}. \qquad (2.29)$$

Both the line sections are terminated by the radiation impedance Z_r.

The input impedance of the equivalent circuit with series voltage source V_{os} can be written as

$$Z_{in} = Z_1 + Z_2, \qquad (2.30)$$

and the input impedance seen by the primary feed line is obtained dividing (2.30) by square of turns ratio, n^2 as follows

$$Z_{in}^F = \frac{Zin}{n^2}, \qquad (2.31)$$

where, n is the turns ratio given by (2.27). The input impedance of the electromagnetically coupled microstrip patch antenna at the feed point is obtained by transforming the input impedance given in equation (2.31) through the low impedance transmission line (feed line) of length L. The required expression for the input impedance of the EMC microstrip patch antenna can be written as

$$Z_{in}^{antenna} = Z_f \frac{Z_{in}^F + j\, Z_f \tan(\beta_f L)}{Z_f + j\, Z_{in}^F \tan(\beta_f L)}, \qquad (2.32)$$

where, Z_f is the characteristic impedance of the feed line and β_f is the propagation constant of the feed line.

2.5 Conclusion

The transmission line model is presented to determine the input impedance of an electromagnetically coupled microstrip patch antenna over two-layer substrates. The advantage of this model lies in its simplicity, that means the input impedance is given by the simple formula (2.32). By using (2.32) a program can be written to give the input impedance for a given set of design parameters (i.e. patch dimensions, frequency, feed length and feed inset). From the input impedance data other performance characteristics such as resonant frequency, bandwidth, input resistance at resonant, and return loss of the antenna can be determined.

Although this model is simple conceptually and computationally, it has some limitations [25]. These are:

(i) the method is useful for rectangular patch only,

(ii) the method cannot be applied to higher order modes, and

(iii) the mutual coupling between the radiating slots is ignored.

In the next chapter a more versatile method is presented to analyze an EMC microstrip patch antenna.

3. CAVITY MODAL ANALYSIS

3.1 Introduction

In the preceding chapter an electromagnetically coupled (EMC) rectangular microstrip patch antenna on two-layered substrates was analyzed using the transmission line model. However, the method has some limitations. A more accurate and versatile method should be invoked to analyze the EMC microstrip patches.

In this chapter the cavity modal analysis is presented for an EMC microstrip patch. In this method, the microstrip patch is viewed as a thin cavity, supporting only the TM_Z-mode, with magnetic walls at its periphery and electric walls at the top and at the bottom. The tangential magnetic field is zero along the fictitious magnetic wall. Similarly, the tangential electric field is zero along the electric wall. The electric fields inside the cavity is expressed as a summation of orthogonal eigenfunctions in an analogous manner of the modal expansion techniques [26]. Each eigenfunction corresponds to a cavity resonant mode and the corresponding eigenvalue is associated with the resonant frequency of the particular mode.

The feed line source excites the fields inside the patch cavity. The source can be attributed, through Huygens' principle, to an equivalent magnetic surface current source. The Helmholtz equation with the source term is solved to calculate the fields in the cavity.

3.2 Cavity Model of Microstrip Patch

When an oscillating current is injected into a microstrip element a charge distribution is established [2] on the surface of the ground plane and on the two surfaces (upper and lower) of the patch as illustrated in figure-3.1(a). There are two opposing tendencies which shape this charge distribution. (1) There is an attractive tendency between the opposite charges at corresponding points on the lower side of the patch and on the ground plane. This attraction tends to keep the patch charge concentrated on the bottom surface of the patch. (2) However, there is also a repulsive tendency between like charges on the bottom of the patch. This tends to push some of the charge around the edge of the patch onto its top surface. When the element is very thin (which is the usual case) the first tendency dominates and almost all the charge on the patch resides on its bottom side. Correspondingly, most of the current flows on the lower side of the patch, with only a small amount of current flowing around the edge onto its upper surface. Specifically, the components of the magnetic field tangential to the patch edge is small although not exactly zero. Were it precisely zero one could introduce a perfect magnetic conductor in the plane between the patch and the ground plane without effecting the fields under the patch. The introduction of such a magnetic wall will distort the shape of the magnetic field distribution.This distortion is negligible if the element is thin. Thus to find the shape of the magnetic field distribution under the patch, one can replace the antenna by an ideal cavity as illustrated in figure-3.1(b). Of course, from the magnetic field distribution the corresponding electric field distribution can also be found.

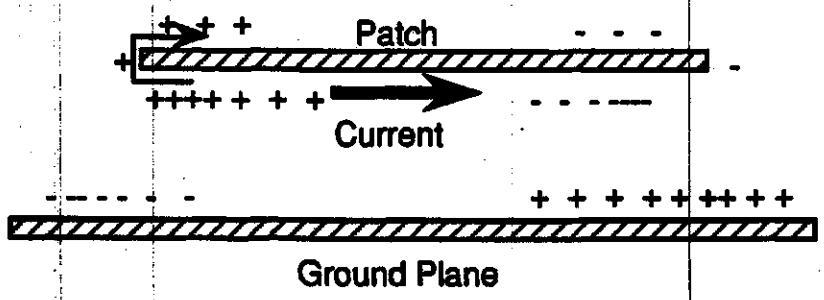

Figure 3.1(a) Charge distribution of the patch

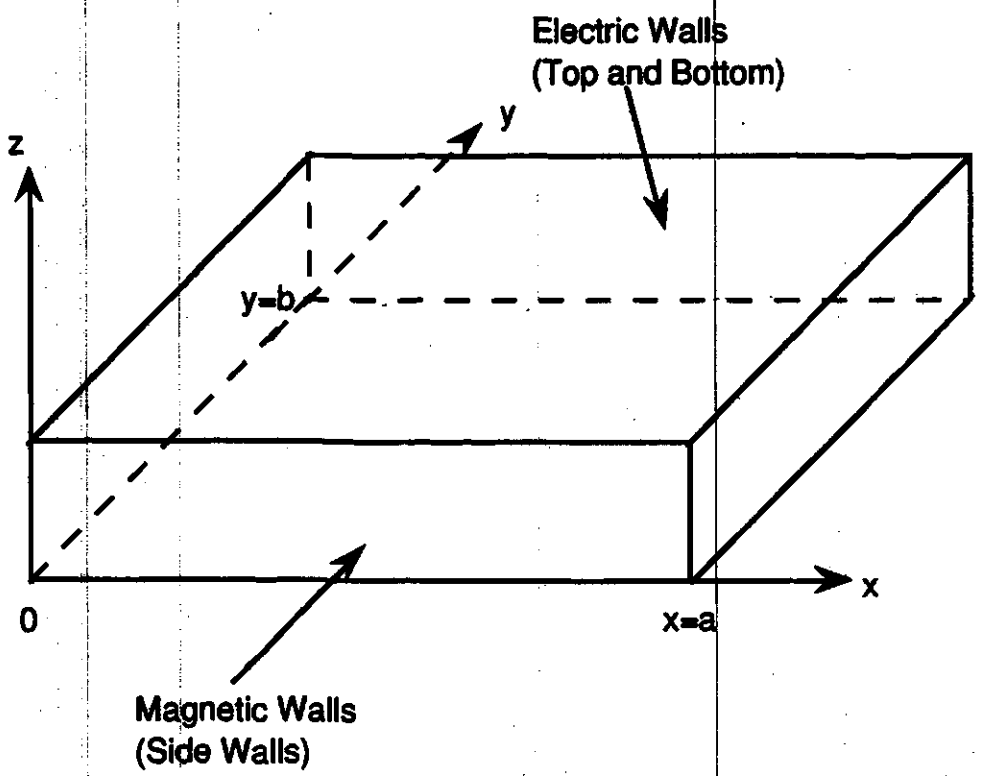

Figure 3.1(b) Cavity model of a patch

Figure-3.1 Cavity model of a typical rectangular microstrip patch antenna

3.3 Modal Expansion Method

In this method a patch is considered to be a thin rectangular cavity resonator. To derive expressions for the fields inside the resonator, the following assumptions [27] are made:

i) the small thickness of the dielectric substrate between the microstrip conductor and the ground plane suggests that only the z-component of the electric field E, and the x- and y-components of the magnetic fields H [see figure-3.1(b)] exist in the region bounded by the microstrip patch and the ground plane,

ii) the fields in the region do not depend on the z-coordinate for all frequencies of interest,

iii) the electric current in the microstrip conductor does not have components normal to the patch edge at any point on the edge, which implies a negligible tangential component of H along the edge.

In order to account for the fringing fields, the magnetic wall is placed slightly away from the periphery (see figure-2.3).

3.3.1 The Helmholtz Equation with Source

The cavity is assumed to be lossless with a perfect magnetic wall in its periphery. The assumption is equally applicable to a microstrip feed line that can be thought of as a small waveguide into the large patch cavity (see figure-3.2). The feed source in the patch cavity may be modeled, by using

Huygens' principle by a strip of y-directed magnetic volume current ($\vec{M} = \vec{E} \times \hat{n}$) backed by a magnetic wall at x=c, between the edge of the feed line and the ground plane. In the ideal case, the feed source can be assumed to be a uniform current ribbon of constant current $\vec{M}$. Fringing of the feed line field (E_z) indicates that the width of the current ribbon is the effective width of the feed line. Thus it is assumed that the cavity is excited by a surface current source located at x = c as shown in figure-3.2. The above excitation can be expressed in terms of feed line field

$$\vec{M} = \vec{E} \times \hat{n}|_{x=c}$$

$$= \begin{cases} E_0 \delta(x-c)\, \hat{y} & \text{for } b/2-w/2 \le y \le b/2+w/2,\ 0 \le z \le d,\ 0 \le x \le a \\ 0, & \text{otherwise} \end{cases} , \qquad (3.1)$$

where, δ is the Dirac-delta function of x at x=c and $\hat{n}$ is the unit normal on the magnetic wall between the edge of the feed line and ground plane. The uniform z-directed electric field between the spaceing of the feed line and the ground plane is given by

$$\vec{E} = \begin{cases} E_0 \hat{z} & \text{for } b/2-w/2 \le y \le b/2+w/2,\ 0 \le z \le d,\ 0 \le x \le a \\ 0 & \text{otherwise} \end{cases} . \qquad (3.2)$$

Maxwell's equations for the magnetic current source only ($\vec{J} = 0$) are as follows

$$\vec{\nabla} \times \vec{H} = j\omega\varepsilon\vec{E} , \qquad (3.3)$$

$$\vec{\nabla} \times \vec{E} = -\vec{M} - j\omega\mu\vec{H} . \qquad (3.4)$$

The electric field in terms of electric vector potential can be written as

$$\vec{E} = -\vec{\nabla} \times \vec{F}. \tag{3.5}$$

Operating a curl on both sides of equation (3.5) and substituting for the same into equation (3.4) yields

$$\vec{\nabla} \times \vec{E} = -(\vec{\nabla} \times \vec{\nabla} \times \vec{F}) = -(\vec{M} + j\,\omega\mu\vec{H}),$$

or,

$$\vec{\nabla}(\vec{\nabla} \cdot \vec{F}) - \nabla^2\vec{F} = \vec{M} + j\omega\mu\vec{H}. \tag{3.6}$$

Equating (3.3) and (3.5) yields the expression for $\vec{E}$ in terms of $\vec{H}$

$$-\vec{E} = \vec{\nabla} \times \vec{F} = -\frac{\vec{\nabla} \times \vec{H}}{j\omega\epsilon}, \tag{3.7}$$

and taking off the curl from both sides of (3.7) yields

$$\vec{F} = -\vec{\nabla}\psi_m - \frac{\vec{H}}{j\omega\epsilon}, \tag{3.8}$$

where, ψ_m is the scalar magnetic potential.

From equation (3.8) the magnetic field can be written as

$$-\vec{H} = j\omega\epsilon(\vec{\nabla}\psi_m + \vec{F}). \tag{3.9}$$

Substituting for this expression of $\vec{H}$ into (3.6) yields

$$\vec{\nabla}(\vec{\nabla} \cdot \vec{F}) - \nabla^2\vec{F} = \vec{M} + \omega^2\mu\epsilon(\vec{\nabla}\psi_m + \vec{F}). \tag{3.10}$$

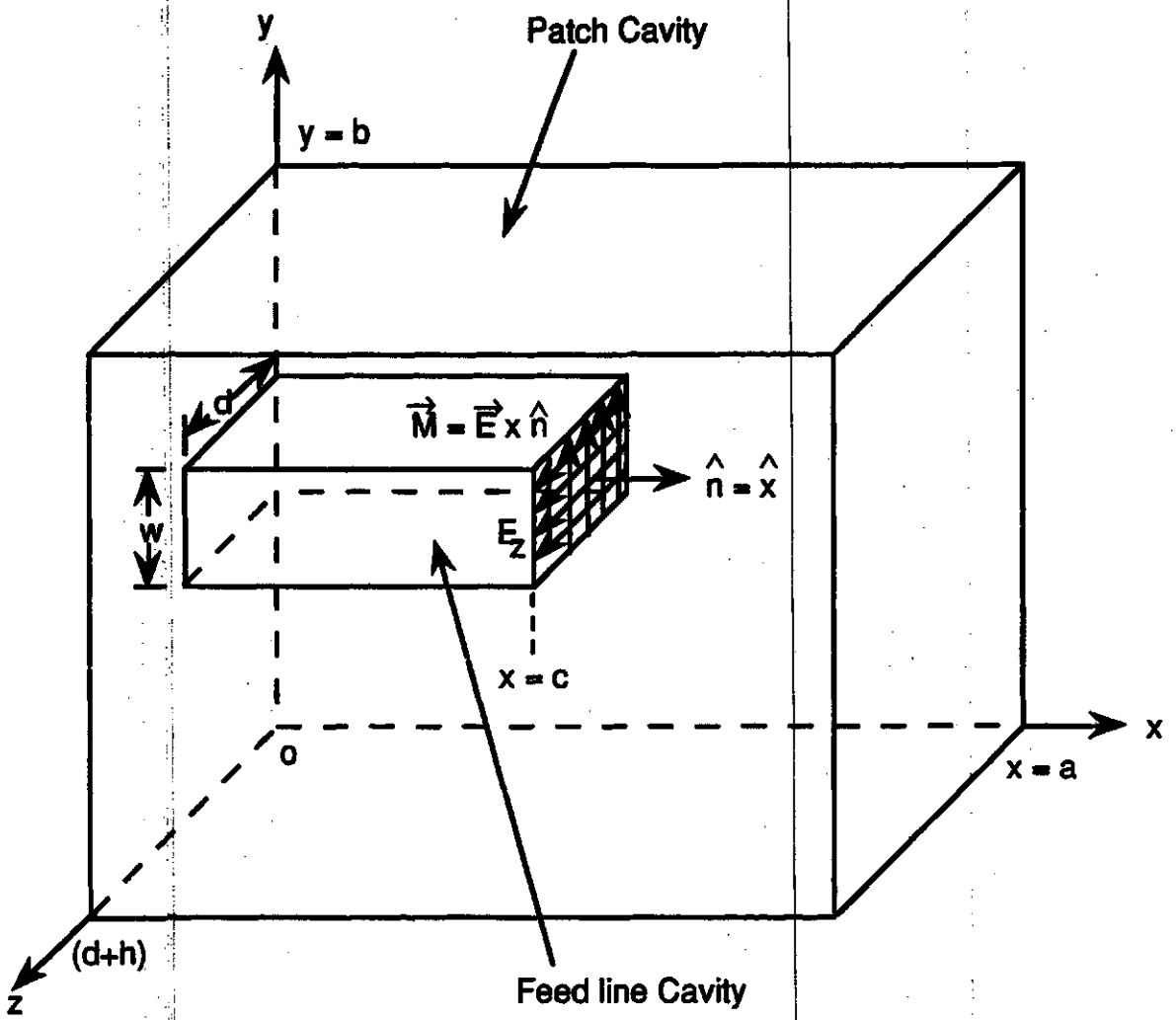

Figure-3.2 Cavity representation of the patch and the feed line

Let $\omega^2\mu\varepsilon\vec{\nabla}\psi_m = \vec{\nabla}(\vec{\nabla}.\vec{F})$ [18], which is known as the Lorentz condition. Using the condition in equation (3.10) yields

$$-\nabla^2\vec{F} = \vec{M} + \omega^2\mu\varepsilon\vec{F},$$

or,

$$\nabla^2\vec{F} + k^2\vec{F} = -\vec{M}. \qquad (3.11)$$

where, $k^2 = \omega^2\mu\varepsilon$ is the propagation constant in the cavity. This equation is known as the inhomogeneous Helmholtz equation. This wave equation of the electric vector potential $\vec{F}$ due to the feed source $\vec{M}$ is the governing equation that determines the modal fields inside the cavity.

When a microstrip patch is fed by a microstrip transmission line, many modal waves are produced in general [27]. The wave equation for $\vec{F}$ in the cavity with excitation current $\vec{M} = E_0\,\delta(x-c)\,\hat{y}$ is (a time dependance of $e^{j\omega t}$ is understood) given by equation (3.11). Since $\vec{M}$ has only y-directed component, the vector electric potential expressed in (3.11) also has only a y-directed component and the expression in (3.11) is simplified to

$$\nabla^2 F_y + k^2 F_y = -M_y. \qquad (3.12)$$

Expression (3.12) is the required wave equation of cavity source. The cavity mode eigenfunction will be determined with the wave equation.

3.3.2 Modal Expansion of the Cavity Fields

The cavity model of a patch antenna consists of two electric walls separated by a magnetic wall around its periphery (see figure-3.1). The radiation pattern, input impedance and radiated power can be calculated based on the traditional approach used for a resonant cavity problems [28]. Since the spacing between the patch and the ground plane is very small, the only component of $\vec{E}$ is in the z-direction and the components of $\vec{H}$ are traverse to z-direction. The cavity is coupled to the microstrip feed line through a narrow magnetic wall containing an unknown field component (E_z) at the end of the feed line. Because of the resulting equivalent magnetic current $\vec{M}$ has only the y component, a field expansion TE to the y-direction will be used. In terms of magnetic and electric vector potentials, the homogeneous vector Helmholtz equations are:

$$\nabla^2 \vec{A} + k^2 \vec{A} = 0, \tag{3.13}$$

$$\nabla^2 \vec{F} + k^2 \vec{F} = -0, \tag{3.14}$$

where, $k = \omega\sqrt{\mu\varepsilon}$, $\varepsilon = \varepsilon_0 \varepsilon_{eff}$ and ε_{eff} is the effective dielectric constant of the substrate given in (2.13).

For the TE to y modes, $\vec{A} = 0$ and $\vec{F} = \hat{y} F_y$, where $\hat{y}$ is a unit vector in the y-direction and F_y is the magnitude of the electric vector potential expressed in (3.14). The $\vec{E}$ and $\vec{H}$ fields are determined from

$$\vec{E} = -\vec{\nabla} \times \vec{F}, \tag{3.5}$$

and,

$$\vec{H} = -j\omega\varepsilon \vec{F} + \frac{1}{j\omega\mu} \vec{\nabla}(\vec{\nabla}.\vec{F}). \tag{3.15}$$

Solving for equations (3.5) and (3.15) yields the field components

$$E_x = \frac{\partial F_y}{\partial z}, \qquad H_x = \frac{1}{j\omega\mu} \frac{\partial^2 F_y}{\partial x \partial y}, \tag{3.16}$$

$$E_y = 0, \qquad H_y = \frac{1}{j\omega\mu}\left[\frac{\partial^2}{\partial y^2} + k^2\right] F_y, \tag{3.17}$$

$$E_z = -\frac{\partial F_y}{\partial x}, \qquad H_z = \frac{1}{j\omega\mu} \frac{\partial^2 F_y}{\partial y \partial z}. \tag{3.18}$$

The modal fields in the cavity must satisfy the wave equation (3.14) and the following boundary conditions [29]:

$$H_x = 0 \qquad \text{at } y = 0 \text{ and } y = b, \tag{3.19}$$

$$H_y = 0 \qquad \text{at } x = 0 \text{ and } x = a, \tag{3.20}$$

$$\frac{\partial E_z}{\partial x}(x=0) = \frac{\partial E_z}{\partial x}(x=a) = 0, \tag{3.21}$$

$$\frac{\partial E_z}{\partial y}(y=0) = \frac{\partial E_z}{\partial y}(y=b) = 0. \tag{3.22}$$

A solution to the wave equation can be found by choosing [30]

$$F_y = (A_x \sin k_x x + B_x \cos k_x x)(A_y \sin k_y y + B_y \cos k_y y) \times (A_z \sin k_z z + B_z \cos k_z z), \tag{3.23}$$

and,

$$k^2 = k_x^2 + k_y^2 + k_z^2. \tag{3.24}$$

The unknowns in (3.23) can be found by applying the boundary conditions. The boundary conditions require that the tangential magnetic field components must be zero on the side walls (magnetic walls) and the tangential electric field components must be zero on the top and bottom walls (electric walls). Since the depth of the cavity is very small (a small fraction of a wavelength) the field components can be considered independent of $\hat{z}$ [27]. Considering the z-independency of the field components in equations (3.16) - (3.18) become

$$E_x = 0, \qquad H_x = \frac{1}{j\omega\mu}\frac{\partial^2 F_y}{\partial x \partial y}, \tag{3.25}$$

$$E_y = 0, \qquad H_y = \frac{1}{j\omega\mu}\left[\frac{\partial^2}{\partial y^2} + k^2\right] F_y, \tag{3.17}$$

$$E_z = -\frac{\partial F_y}{\partial x}, \qquad H_z = 0. \tag{3.26}$$

Solving for H_x and H_y yields

$$H_x = \frac{k_x k_y}{j\omega\mu}(A_x \cos k_x x - B_x \sin k_x x)(A_y \cos k_y y - B_y \sin k_y y), \tag{3.27}$$

and

$$H_y = \frac{k^2 - k_y^2}{j\omega\mu}(A_x \sin k_x x + B_x \cos k_x x)(A_y \sin k_y y + B_y \cos k_y y). \tag{3.28}$$

The magnetic fields inside the cavity must satisfy the boundary conditions in (3.19) and (3.20). Applying the boundary conditions into (3.27) yields

$$\text{at } y = 0, \quad H_x = 0 \longrightarrow \quad A_y = 0;$$

$$\text{at } y = b, \quad H_x = 0 \longrightarrow \quad \sin(k_y b) = 0;$$

$$k_y = \left(\frac{n\pi}{b}\right), \quad n = 0,1,2, \ldots\ldots\ldots\ldots . \tag{3.29}$$

Applying the same boundary conditions into (3.28) yields

$$\text{at } x = 0; \quad H_y = 0 \longrightarrow \quad B_x = 0;$$

$$\text{at } x = a; \quad H_y = 0 \longrightarrow \quad \sin(k_x a) = 0;$$

$$k_x = \left(\frac{m\pi}{a}\right), \; m = 0,1,2, 3 \ldots\ldots\ldots\ldots . \tag{3.30}$$

Equation (3.23) can now be reduced to

$$F_y = A_x B_y \sin\left(\frac{m\pi x}{a}\right)\cos\left(\frac{n\pi y}{b}\right) = F_{mn} \sin\left(\frac{m\pi x}{a}\right)\cos\left(\frac{n\pi y}{b}\right), \tag{3.31}$$

where, $F_{mn} = A_x B_y$ are orthogonal mode amplitude coefficients which must be determined. The dominant mode of the cavity can be found from equation (3.24) as follows

$$k_{mn} = \sqrt{\left(\frac{m\pi}{a}\right)^2 + \left(\frac{n\pi}{b}\right)^2}, \tag{3.32a}$$

and,

$$\omega_{mn} = \frac{1}{\sqrt{\mu\varepsilon}} \sqrt{\left(\frac{m\pi}{a}\right)^2 + \left(\frac{n\pi}{b}\right)^2}. \tag{3.32b}$$

For m = 1, n = 0, ω_{10} will be the dominant mode resonant frequency for a patch cavity of length a ≈ λ/2.

In order to find the modal expansion of the fields inside the cavity due to the magnetic current $\vec{M}$ at the edge of the feed line, an eigenfunction expansion is applied to the inside electric field so that the electric fields inside the cavity could be expressed as a Fourier series expansion [21] as follows:

$$\vec{E} = \sum_{mn} \vec{E}_{mn} = -\vec{\nabla} \times \vec{F} = -\hat{z} \frac{\partial F_y}{\partial x} \tag{3.33}$$

The electric field inside the cavity must satisfy the wave equation (3.11) and the cavity wall boundary conditions given in equations (3.21) and (3.22). An eigenfuncition expansion of the electric vector potential F_y in (3.31) can be written as

$$F_y = \sum_{mn} F_{mn} \sin(\frac{m\pi x}{a})\cos(\frac{n\pi y}{b}), \tag{3.34}$$

where, F_{mn} are the mode amplitude coefficients of the electric vector potential inside the cavity.

Substitution for F_y from equation (3.34) into equation (3.33), the z-directed electric field component inside the cavity can be written as

$$E_z = -\sum_{mn} F_{mn}(\frac{m\pi}{a}) \cos(\frac{m\pi x}{a}) \cos(\frac{n\pi y}{b}). \tag{3.35}$$

To determine the field components, the factor F_{mn} must be found. By substitution for F_y from equation (3.34) into equation (3.12) yields

$$\sum_{m\,n} F_{mn}\left[\frac{\partial^2}{\partial x^2}\left\{\sin\left(\frac{m\pi x}{a}\right)\cos\left(\frac{n\pi y}{b}\right)\right\} + \right.$$

$$\left.\frac{\partial^2}{\partial y^2}\left\{\sin\left(\frac{m\pi x}{a}\right)\cos\left(\frac{n\pi y}{b}\right)\right\} + k^2\sin\left(\frac{m\pi x}{a}\right)\cos\left(\frac{n\pi y}{b}\right)\right]$$

$$= -\,M_y. \qquad (3.36)$$

Substitution for the value of M_y from (3.1) into (3.36) yields

$$\sum_{m\,n} F_{mn}\left(k^2 - k_{mn}^2\right)\sin\left(\frac{m\pi x}{a}\right)\cos\left(\frac{n\pi y}{b}\right)$$

$$= \begin{cases} E_0\,\delta(x-c)\,\hat{y} & \text{for } b/2-w/2 \le y \le b/2+w/2,\ 0 \le z \le d,\ 0 \le x \le a \\ 0 & \text{otherwise} \end{cases}, \qquad (3.37)$$

where, k_{mn} is the TM_{mn} modes eigenvalue given in (3.32a).

Multiplying both sides of (3.37) by $\sin\left(\frac{m\pi x}{a}\right)\cos\left(\frac{n\pi y}{b}\right)$ and integrating over the entire patch cavity $0 \le x \le a$ and $0 \le y \le b$, $0 \le z \le (d+h)$, (for a particular mn-mode) yields

$$F_{mn}\left(k^2 - k_{mn}^2\right)\int_{x=0}^{a}\sin^2\left(\frac{m\pi x}{a}\right)dx\int_{y=0}^{b}\cos^2\left(\frac{n\pi y}{b}\right)dy\int_{z=0}^{(d+h)}dz$$

$$= -E_0\int_{x=0}^{a}\delta(x-c)\sin\left(\frac{m\pi x}{a}\right)dx\int_{y=b/2-w/2}^{b/2+w/2}\cos\left(\frac{n\pi y}{b}\right)dy\int_{z=0}^{d}dz,$$

or,

$$F_{mn} = -8E_0 \frac{d \sin(\frac{m\pi c}{a})\sin(\frac{n\pi w}{2b}) \cos(\frac{n\pi}{2})}{a(d+h)\ n\pi(k^2 - k_{mn}^2)\varepsilon_m \varepsilon_n}, \qquad (3.38)$$

where, ε_n is given by

$$\varepsilon_n = \begin{cases} 2, & \text{for } n = 0 \\ 1, & \text{for } n \neq 0 \end{cases}$$

The electric vector potential is obtained by substituting for (3.38) into equation (3.34) as

$$F_y = -8E_0 \frac{d}{\pi a(d+h)} \times$$

$$\sum_{m\,n} \frac{\sin(\frac{m\pi c}{a})\ \sin(\frac{n\pi w}{2b})\ \cos(\frac{n\pi}{2})\ \sin(\frac{m\pi x}{a})\cos(\frac{n\pi y}{b})}{n(k^2 - k_{mn}^2)\varepsilon_m \varepsilon_n} \qquad (3.39)$$

The fields inside the patch cavity are then readily obtained by using equation (3.39) into equations (3.35) and (3.17), where

$$E_z = 8E_0 \frac{d}{\pi a(d+h)} \times$$

$$\sum_{m\,n} \frac{\sin(\frac{m\pi c}{a})\sin(\frac{n\pi w}{2b})\ \cos(\frac{n\pi}{2})}{n(k^2 - k_{mn}^2)\varepsilon_m \varepsilon_n} (\frac{m\pi}{a})\cos(\frac{m\pi x}{a})\cos(\frac{n\pi y}{b}), \qquad (3.40)$$

and,

$$H_y = \frac{1}{j\omega\mu}\{-8E_0 \frac{d}{\pi a(d+h)}\} \times$$

$$\sum_{m\,n} \frac{\sin(\frac{m\pi c}{a})\sin(\frac{n\pi w}{2b})\cos(\frac{n\pi}{2})}{n(k^2 - k_{mn}^2)\varepsilon_m \varepsilon_n} (k^2 - k_y^2)\sin(\frac{m\pi x}{a})\cos(\frac{n\pi y}{b}). \quad (3.41)$$

The determination of the fields inside the patch cavity is now completed here. Using these fields, the stored power inside the cavity and the radiated power out from the cavity can be found. From the total power inside the cavity the input impedance is formulated.

The remaining task is to solve for the input impedance for the dominant mode which is TM_{10} (m = 1, n = 0) mode inside the patch cavity [2].

3.4 Input Impedance of TM_{10} Cavity Mode

The fields in the patch cavity for the particular dominant mode are found to determine the input impedance of the patch antenna. Starting with the expression for the electric vector potential F_y in equation (3.34) for m = 1 and n = 0 at TM_{10} dominant cavity mode one obtains:

$$F_y = F_{10} \sin(\frac{\pi x}{a}). \quad (3.42)$$

The dominant mode eigenvalue and the resonant frequency in equation (3.32) becomes

$$k_{10} = \frac{\pi}{a}, \quad (3.43a)$$

$$\omega_{10} = \frac{1}{\sqrt{\mu\varepsilon}}(\frac{\pi}{a}). \quad (3.43b)$$

Substituting for equation(3.42) into equation (3.37) yields

$$F_{10}[k^2 - (\frac{\pi}{a})^2] \sin(\frac{\pi x}{a})$$

$$= \begin{cases} E_0 \delta(x-c)\,\hat{y} \text{ for } b/2-w/2 \le y \le b/2+w/2,\ 0 \le z \le d,\ 0 \le x \le a \\ 0 \quad \text{otherwise} \end{cases} \qquad (3.44)$$

Multiplying both sides of (3.44) with $\sin(\frac{\pi x}{a})$ and integrating over the entire patch cavity yields

$$F_{10}[k^2 - (\frac{\pi}{a})^2] \int_{x=0}^{a} \sin^2(\frac{\pi x}{a})dx \int_{y=0}^{b} dy \int_{z=0}^{(d+h)} dz$$

$$= -E_0 \int_{x=0}^{a} \delta(x-c) \sin(\frac{\pi x}{a})\,dx \int_{y=b/2-w/2}^{b/2+w/2} dy \int_{z=0}^{d} dz\,,$$

or,

$$F_{10} = -2E_0 \frac{wd \sin(\frac{\pi c}{a})}{ab(d+h)\{k^2 - (\frac{\pi}{a})^2\}}. \qquad (3.45)$$

From the vector electric potential in equation (3.41) the electric field inside the cavity can be found by using equation (3.5). The z-directed electric field inside the cavity for TM_{10} mode can be written as

$$E_z = E_{10} = -\frac{\partial F_y}{\partial x}$$

$$= -F_{10}(\frac{\pi}{a}) \cos(\frac{\pi x}{a}). \qquad (3.46)$$

The magnetic field in the patch cavity can be found by using equation (3.17) (where $\partial/\partial y = 0$), and for the dominant mode can be written as

$$H_y = -j\omega\varepsilon F_{10} \sin(\frac{\pi x}{a}) . \qquad (3.47)$$

Given the inside field components in equations (3.46) and (3.47) the complex power inside the cavity and the radiation real power are found. The total power supplied by the magnetic current source is the summation of these two powers. From the total power the input impedance of the EMC patch antenna is formulated.

The stored power into the cavity is given by [21]:

$$P_s = -\int_v H_y^* M_y \, dv = -j2\omega\varepsilon E_0^2 \frac{w\, d \sin(\frac{\pi c}{a})}{ab(d+h)\{k2-(\frac{\pi}{a})^2\}}$$

$$\int_{x=0}^{a} \delta(x-c) \sin(\frac{\pi x}{a}) \, dx \int_{y=(b-w)/2}^{(b+w)/2} dy \int_{z=0}^{d} dz$$

or,

$$P_s = -j2\omega\varepsilon E_0^2 \frac{w^2 d^2 \sin^2(\frac{\pi c}{a})}{ab(d+h)\{k2-(\frac{\pi}{a})^2\}} \qquad (3.48)$$

where, M_y is the magnetic current at the feed end given in equation (3.1). The above equation gives the power for the particular dominant mode and in the present case it is imaginary.

The real power is the radiation power that gives the radiation loss. The radiation power can be found by considering the microstrip cavity has two edges (magnetic walls) at a distance a in the y-z plane. For the dominant TM_{10} mode, the variation of E_Z along y-axis is constant and along x-axis is sinusoidal. In this mode the magnetic currents on two opposite edges are constant [2]. These edges are called the radiation edges. The magnetic currents on the remaining two edges suffer a phase reversal and hence the fields radiated by them largely cancel. The fields at the radiation edges at x=0 and x = a can be written as

$$E_z(x=0) = -F_{10}\left(\frac{\pi}{a}\right), \tag{3.49}$$

and,

$$E_z(x=a) = F_{10}\left(\frac{\pi}{a}\right). \tag{3.50}$$

The voltage drop across the radiation edges can be written as

$$V_0(x=0) = (d+h)E_z(x=0), \tag{3.51}$$

and,

$$V_0(x=a) = (d+h)E_z(x=a). \tag{3.52}$$

The total radiated power from the two edges is derived in equation (2.6) and can now be written as

$$P_r = \frac{V_o^2 I_1}{120\pi^2}$$

$$= \frac{E_0^2}{30}\left(\frac{wd}{ab}\right)^2 \sin^2\left(\frac{\pi c}{a}\right) \frac{I_1}{a^2\{k^2-(\frac{\pi}{a})^2\}^2}. \qquad (3.53)$$

Total power supplied by the source for the dominant TM_{10} mode is the sum of (3.48) and (3.53)

$$P_t = P_r + P_s$$

$$= \frac{E_0^2}{60}\left(\frac{wd}{ab}\right)^2 \frac{\sin^2\left(\frac{\pi c}{a}\right)}{a^2\{k^2-(\frac{\pi}{a})^2\}^2} [2I_1 - j\frac{k}{\pi}\sqrt{\varepsilon_{eff}}\frac{ab}{(d+h)} a^2\{k^2-(\frac{\pi}{a})^2\}].$$

(3.54)

The input admittance, as seen by the feed line at its end, in the patch cavity is :

$$Y_{10} = \frac{P_t}{|\, dE_0 \,|^2}$$

$$= \frac{1}{60}\left(\frac{w}{ab}\right)^2 \frac{\sin^2\left(\frac{\pi c}{a}\right)}{a^2\{k^2-(\frac{\pi}{a})^2\}^2} [\, 2I_1 - j\frac{k}{\pi}\sqrt{\varepsilon_{eff}}\frac{ab}{(d+h)} a^2\{k^2-(\frac{\pi}{a})^2\}]. \qquad (3.55)$$

The input impedance is the reciprocal of equation (3.55) and is given by

$$Z_{10} = \frac{1}{Y_{10}} \qquad (3.56)$$

The equation (3.56) is the required expression for the input impedance of the electromagnetically coupled microstrip patch antenna for the dominant TM_{10} cavity mode. By using transmission line equation in (2.32), transforming the above impedance through the low impedance

transmission line (feed line) the input impedance, as seen at the feed point of the antenna, will be obtained.

3.5 Conclusion

Electromagnetically coupled microstrip patch antenna has been analyzed using cavity modal theory. The dominant mode into the resonant patch cavity is the TM_{10} mode. The total power supplied by the feed line is the summation of the radiation power out from the patch cavity and the reactive stored power in the cavity. By using the total power supplied by the magnetic current source, the input impedance seen by the feed line is formulated in equations (3.55) and (3.56). A computer program is written with the expressions in equations (3.55) and (3.56) to calculate the input impedance for different frequencies and patch dimensions. The other characteristic parameters are also found from the input impedance data. The results will be shown in chapter-5.

Although this method is versatile compared to the transmission line model in geometrical aspect and is also applicable to other geometries, it suffers from the following limitations [25]:

(1) The model is valid for thin dielectric substrate only.

(2) The model cannot include the effect of the mutual coupling on the aperture fields when there are more than one radiating aperture.

(3) The cavity model gives the field distributions compared to that of standing waves. The standing wave distribution occurs in case of resonant type patches ($a \approx \lambda/2$). In the case of a travelling wave

antenna, the field distribution is of progressive type, and therefore cannot be determined by cavity model.

In the following chapter a more generalized method will be presented.

4. PLANAR WAVEGUIDE MODEL

4.1 Introduction

In the preceding two chapters electromagnetically coupled (EMC) microstrip patch antennas were analyzed utilizing the transmission line model and the cavity modal respectively. The advantages and disadvantages of these two methods were also discussed in the concluding remarks of the relevant chapters. This chapter proposes a more generalized method to analyze the EMC microstrip patch antennas [31].

The present analysis of the EMC patch antenna utilizes the concept of *waveguide excitation* [24]. The antenna structure is considered to be a rectangular planar waveguide bounded by electric and magnetic walls. A microstrip probe (feed line) is inserted in the waveguide to excite it. The overlap region of the feed line and patch antenna contains the source of waveguide excitation. The primary electric field over the feed line is assumed to be z-directed. The transition of RF power from the feedline to the waveguide is due to the fringe electric fields. The equivalent magnetic current of the fringe electric fields is, therefore, the primary source of antenna excitation. In the analysis the waveguide is assumed to be infinitely long in both directions. Invoking the reciprocity theorem, the equivalent circuit of the feed-patch transition in the overlap is determined first. Then the complete equivalent circuit of the EMC microstrip antenna is readily obtained by adding the effects of the radiating edges of the patch. The transition (coupling) of the microstrip feed line and the microstrip

radiating element (patch) is represented by an ideal transformer. The input impedance of the antenna is determined from the equivalent circuit. From the input impedance data, the characteristic features of the antenna are extracted.

4.2 Formulation

Consider a rectangular microstrip patch antenna excited by an open ended microstrip feed line (see figure-4.1). The feed line is located at the interface of two dielectric layers. The relative dielectric constants of the upper and lower layers are ε_h and ε_d respectively. The thickness of the upper dielectric layers is h and and that of the lower one is d. The length and the width of the feed line are L and w respectively of which length c is the feed inset (overlap) under the patch. The length of the radiating patch is a and the width is b. The feed line is centered with respect to the patch width. Since the coupling is primarily due to the fringing electric field (for an open ended microstrip line, the magnetic field is negligible near the edge of the patch), it is, therefore, justified to consider an equivalent magnetic surface current as the primary source of antenna excitation. The equivalent magnetic current is obtained once the electric field of the feed line is known. The electric field between the feed line and the ground plane is given by

$$E_{zf} = E_0 \frac{\cos\{\beta_f(x-c)\}}{\cos(\beta_f c)}, \qquad (4.1)$$

where, E_0 is the z-directed electric field at x=0, β_f is the propagation constant of the microstrip feed line and c is the feed inset under the patch.

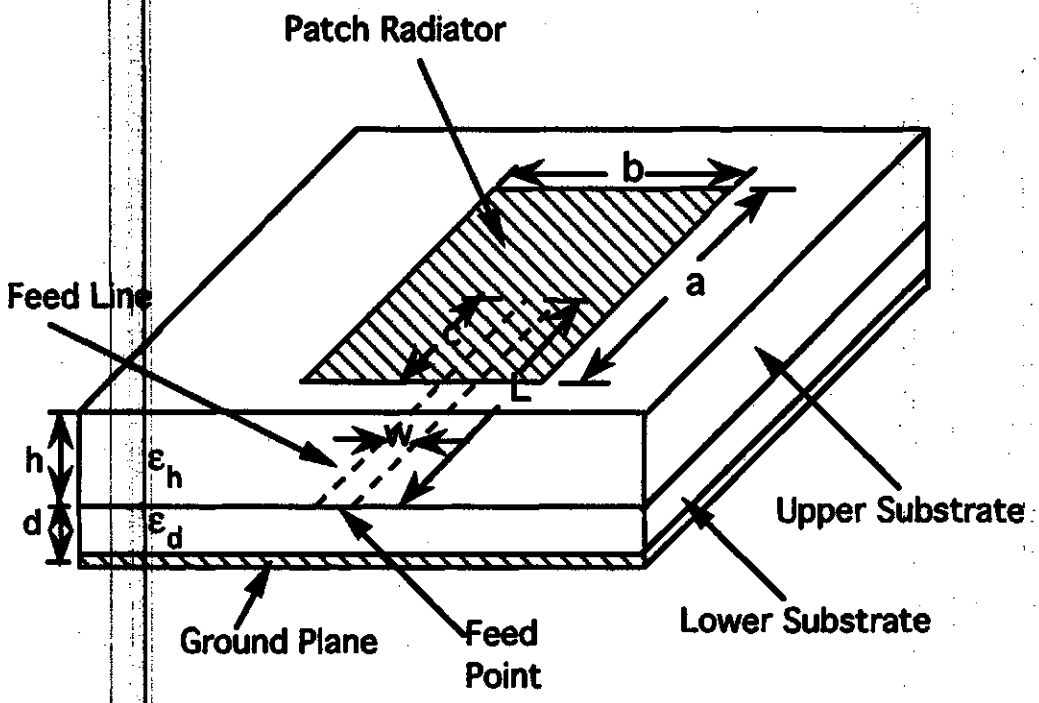

Figure-4.1 A two-layer electromagnetically coupled microstrip patch antenna

Using Huygens' principle, the equivalent magnetic volume current due to the fringing of the primary electric field at x=c (between the edge of the feed line and the ground plane) is found. This magnetic current backed by a magnetic wall at x=c is considered to be the primary source of antenna excitation and is given as follows:

$$\vec{M}_1 = E_{zf}\,\hat{z}\times\hat{n}$$

$$= \begin{cases} \dfrac{E_0\,\delta(x-c)}{\cos(\beta_f c)}\hat{y} & \text{for } \dfrac{b-w}{2} \le y \le \dfrac{b-w}{2},\ 0 \le x \le a,\ 0 \le z \le d \\ 0 & \text{otherwise} \end{cases} , \qquad (4.2)$$

where, $\hat{n}$ is the unit normal over the magnetic wall at x=c and for this case $\hat{n} = \hat{x}$.

In order to make the analysis simple, the equivalent circuit of the feed line and the microstrip patch (of width b) transition are developed first. Once the equivalent circuit is obtained, the effect of the radiating edges can be incorporated properly. In the development of the equivalent circuit of the transition, the microstrip planar waveguide is assumed to be infinitely long in both directions. Figure-4.2 illustrates an infinitely long rectangular

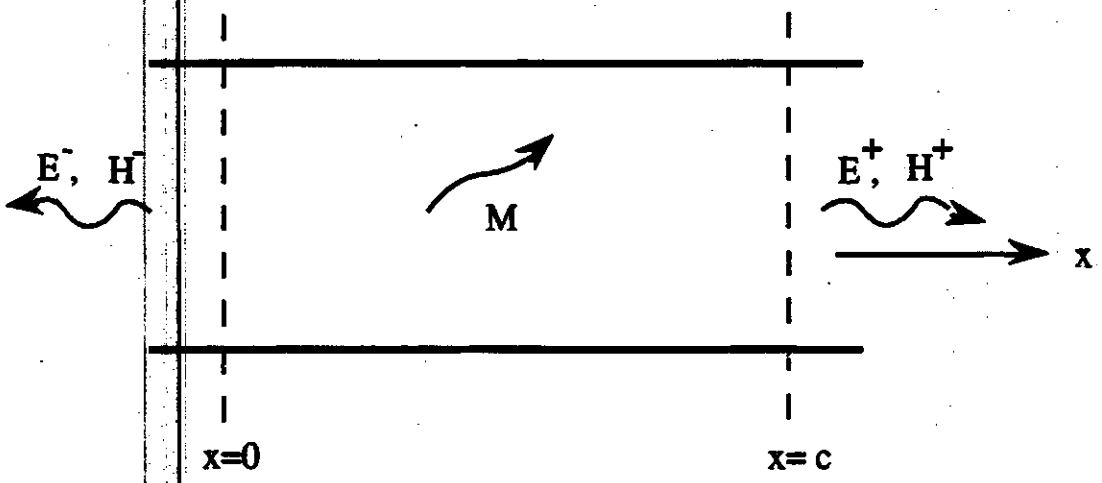

Figure-4.2 Planar waveguide representation of feedline-patch overlap with magnetic current source $\vec{M}$ (Top view)

planar waveguide in which a current source $\vec{M}$ is located in the region between x=0 and x=c. The electromagnetic field radiated by this source may be expressed as an infinite sum of waveguide modes [24] as follows:

$$\vec{E}^{+} = \sum_{n} C_n^{+} \left[e_z \, \hat{z} + e_x \, \hat{x} \right] e^{-jk_x x}, \quad x > c \tag{4.3a}$$

$$\vec{H}^{+} = \sum_{n} C_n^{+} h_y \hat{y} e^{-jk_x x}, \quad x > c \tag{4.3b}$$

$$\vec{E}^{-} = \sum_{n} C_n^{-} [e_z \hat{z} - e_x \hat{x}] e^{+jk_x x}, \quad x < 0 \tag{4.3c}$$

$$\vec{H}^{-} = \sum_{n} - C_n^{-} h_y \hat{y} e^{+jk_x x}, \quad x < 0 \tag{4.3d}$$

where, C_n^{+} and C_n^{-} are the mode amplitude coefficients of the fields $\vec{E}^{+}$, $\vec{H}^{+}$ and $\vec{E}^{-}$, $\vec{H}^{-}$ respectively for n-th mode.

The electromagnetic fields for transverse electromagnetic (TEM) modes propagating underneath of a two-layer wide microstrip patch are given by

$$E_z = D_1 e_z e^{-jk_x x}, \tag{4.4a}$$

$$E_x = D_1 e_x e^{-jk_x x}, \tag{4.4b}$$

$$H_y = D_1 h_y e^{-jk_x x}, \tag{4.4c}$$

where, D_1 is the mode amplitude coefficient and e_z, e_x, h_y are the orthonormal field mode vector components for the electric and magnetic fields respectively. k_x is the propagation constant of a two-layer microstrip transmission line. The expressions for the above quantities are given by [21]

$$e_z = \frac{f(z)}{\varepsilon(z)}, \tag{4.5}$$

$$h_y = -\omega \frac{f(z)}{k_x}, \tag{4.6}$$

$$k_x = k_0 \sqrt{\varepsilon_{eff}}, \tag{4.7}$$

where, k_0 is the propagation constant in the free space and ε_{eff} is the effective permittivity of the two-layer substrates given in (2.13).

The functions $\varepsilon(z)$ and $f(z)$ are defined as follows:

$$\varepsilon(z) = \begin{cases} \varepsilon_0\varepsilon_d & 0 < z < d \\ \varepsilon_0\varepsilon_h & d < z < d+h \end{cases}, \tag{4.8}$$

and,

$$f(z) = \begin{cases} \cos(k_{dz}z), & 0 < z < d \\ \cos(k_{hz}(z-d-h)\dfrac{\cos(k_{dz}d)}{\cos(k_{hz}h)}, & d < z < d+h \end{cases}, \tag{4.9}$$

where, k_{dz} and k_{hz} are given by [24]

$$k_{dz} = \sqrt{k_0^2\varepsilon_d - k_x^2}, \tag{4.10a}$$

$$k_{hz} = \sqrt{k_0^2\varepsilon_h - k_x^2}. \tag{4.10b}$$

In order to obtain the equivalent circuit of the microstrip feed line-patch transition, the electromagnetic fields inside the waveguide excited by the magnetic current source $\vec{M}_1$ are to be determined. The reciprocity theorem is invoked to obtain the fields. The theorem is expressed (for $\vec{J} = 0$) as follows [21]:

$$\iint_s (\vec{E}_1 \times \vec{H}_2 - \vec{E}_2 \times \vec{H}_1).d\vec{s} = \int_v (\vec{H}_1.\vec{M}_2 - \vec{H}_2.\vec{M}_1)\, dv, \qquad (4.11)$$

where, $\vec{E}_1, \vec{H}_1$ and $\vec{E}_2, \vec{H}_2$ are two sets of electric and magnetic fields produced by the magnetic current sources $\vec{M}_1$ and $\vec{M}_2$ respectively. In this case $\vec{E}_1, \vec{H}_1$ are considered to be the total fields excited by the equivalent magnetic current source $\vec{M}_1$ inside the waveguide. $\vec{E}_2$ and $\vec{H}_2$ are the auxiliary test fields due to an auxiliary source $\vec{M}_2$. These test fields can be any fields as long as they satisfy Maxwell's equations.

The primary electric field $\vec{E}_1$ is expressed as [24]:

$$\vec{E}_1^{+} = C^{+} [e_z \hat{z} + e_x \hat{x}] e^{-jk_x x}, \; x > c \qquad (4.12a)$$

$$\vec{E}_1^{-} = C^{-} [e_z \hat{z} - e_x \hat{x}] e^{+jk_x x}, \; x < 0 \qquad (4.12b)$$

where C^{+} and C^{-} are the amplitudes of the fields $\vec{E}_1^{+}$ and $\vec{E}_1^{-}$ respectively, which are to be obtained.

The corresponding magnetic field vectors are given as follows:

$$\vec{H}_1^{+} = C^{+} h_y \hat{y} e^{-jk_x x}, \; x > c \qquad (4.13a)$$

$$\vec{H}_1^{-} = -C^{-} h_y \hat{y} e^{+jk_x x}, \; x < 0 \qquad (4.13b)$$

where, h_y is given in (4.6).

In order to solve for the field coefficients C^+ and C^-, the test fields must be chosen. As mentioned earlier, any chosen field can be used as long as it satisfies Maxwell's equations. All boundary conditions must be met, so a field which makes the mathematics as simple as possible is desirable. In this case a field with unit amplitude and the same field configuration as that of the fundamental mode of the waveguide is chosen.

Considering an auxiliary test source at $x = \infty$, and the fields produced by the source are chosen, namely

$$\vec{E}_2 = [e_z \hat{z} + e_x \hat{x}] e^{+jk_x x}, \tag{4.14a}$$

$$\vec{H}_2 = -h_y \hat{y} e^{+jk_x x}. \tag{4.14b}$$

Since the fields $\vec{E}_2$ and $\vec{H}_2$ are a source free solutions ($\vec{M}_2 = 0$) within the waveguide and the surface integral is zero over the waveguide walls by virtue of the boundary conditions: $\hat{n} \times \vec{E}$ (perfect electric walls) = $\vec{H} \times \hat{n}$ (perfect magnetic walls) = 0, equation (4.11) reduces to

$$\iint_{s_1} (\vec{E}_1^- \times \vec{H}_2 - \vec{E}_2 \times \vec{H}_1^-) . \hat{n} \, ds_1$$

$$+ \iint_{s_2} (\vec{E}_1^+ \times \vec{H}_2 - \vec{E}_2 \times \vec{H}_1^+) . \hat{n} \, ds_2 = - \int_v \vec{H}_2 . \vec{M}_1 \, dv , \tag{4.15}$$

where, S_1 and S_2 are the cross-sectional areas of the waveguide at x=0 and x=c respectively and $\hat{n}$ is the unit outward normal on the surface. By making the appropriate substitutions for $\vec{E}_1^+$, $\vec{E}_1^-$, $\vec{H}_1^+$ and $\vec{H}_1^-$, equation (4.15) can be written as

$$\int_{y=0}^{b}\int_{z=0}^{d+h} C^- \{(e_z\hat{z}-e_x\hat{x})\times(-h_y\hat{y}) - (e_z\hat{z}-e_x\hat{x})\times(-h_y\hat{y})\}e^{-j2k_x x}.(\hat{-x})\,dz\,dy$$

$$+ \int_{y=0}^{b}\int_{z=0}^{d+h} C^+ \{(e_z\hat{z}+e_x\hat{x})\times(-h_y\hat{y}) - (e_z\hat{z}-e_x\hat{x})\times(h_y\hat{y})\}.\hat{x}\,dz\,dy$$

$$= -\int_v \vec{H}_2.\vec{M}_1 dv,$$

or,

$$2C^+ \int_{y=0}^{b}\int_{z=0}^{d+h} e_z h_y dz\,dy = \int_v \vec{M}_1.\hat{y}h_y e^{+jk_x x} dv.$$

The unknown mode amplitude coefficient C^+ can now be written as

$$C^+ = \frac{1}{2P_n}\int_v (\vec{M}_1.\hat{y})h_y e^{+jk_x x}\,dv, \qquad (4.16)$$

where,

$$P_n = \int_{y=0}^{b} \int_{z=0}^{d+h} e_z h_y \, dz \, dy. \tag{4.17}$$

In order to determine C^-, another set of equations is available. They are found by considering the negative traveling wave of the test fields. The test fields now become

$$\vec{E}_2 = [\, e_z \hat{z} + e_x \hat{x}] \, e^{-jk_x x}, \tag{4.18a}$$

$$\vec{H}_2 = h_y \hat{y} \, e^{-jk_x x}. \tag{4.18b}$$

Using the same procedure as for the determination of C^+, (4.15) can be written as

$$\int_{y=0}^{b} \int_{z=0}^{d+h} C^- \{(e_z\hat{z}-e_x\hat{x})\times(h_y\hat{y})-(e_z\hat{z}+e_x\hat{x})\times(-h_y\hat{y})\}.(-\hat{x}) \, dz \, dy$$

$$+ \int_{y=0}^{b} \int_{z=0}^{d+h} C^+ \{(e_z\hat{z}+e_x\hat{x})\times(-h_y\hat{y})-(e_z\hat{z}+e_x\hat{x})\times(h_y\hat{y})\} \, e^{-j2k_x x}.\hat{x} \, dz \, dy$$

$$= -\int_v \vec{H}_2 . \vec{M}_1 \, dv,$$

or,

$$2C^{-}\int_{y=0}^{b}\int_{z=0}^{d+h} e_z h_y \, dz\, dy = -\int_{v}\vec{M}_1 \cdot \hat{y} h_y e^{-jk_x x}\, dv,$$

or,

$$C^{-} = -\frac{1}{2P_n}\int_{v}(\vec{M}_1 \cdot \hat{y}) h_y \, e^{-jk_x x}\, dv, \qquad (4.19)$$

where, $\vec{M}_1$ and h_y are given in equations (4.2) and (4.6) respectively.

Solving for the unknown coefficients C^{+} and C^{-} is now a matter of substitutions for $\vec{M}_1$ and h_y only. By making these substitutions and solving for each of the integrals on the right hand side of (4.16) and (4.19) yields

$$C^{+} = \frac{1}{2P_n}\frac{E_0}{\cos(\beta_f c)} wd\left(\frac{-\omega}{k_x}\right) e^{+jk_x c} = AE_0 e^{+jk_x c}, \qquad (4.20)$$

$$C^{-} = -\frac{1}{2P_n}\frac{E_0}{\cos(\beta_f c)} wd\left(\frac{-\omega}{k_x}\right) e^{-jk_x c} = -AE_0 e^{-jk_x c}, \qquad (4.21)$$

where,

$$A = \frac{1}{2P_n}\frac{1}{\cos(\beta_f c)} wd\left(\frac{-\omega}{k_x}\right) \qquad (4.22)$$

Substitutions for the values of C^{+} and C^{-} into (4.12)-(4.13) yield the electric and magnetic fields excited inside the waveguide by the primary source $\vec{M}_1$.

This completes the determination of required fields inside the waveguide. The next step is to determine the z-directed electric field at x=o and x=c, and the corresponding voltages at the two points.

The z-directed electric field component E_z at x=0 and x=c are obtained by substitution for C^+ and C^- from equations (4.20) and (4.21) into equations (4.12) and (4.14) as follows:

$$E_z(x=0) = C^- e_z e^{+jk_x x}\Big|_{x=0} = -E_0 A\, e_z e^{-jk_x c}, \tag{4.23a}$$

$$E_z(x=c) = C^+ e_z e^{-jk_x x}\Big|_{x=c} = E_0 A\, e_z . \tag{4.23b}$$

where, e_z and A are given in equations (4.5) and (4.22) respectively.

Form (4.23) it is observed that the transverse electric field across the source (overlap) is discontinuous.

The voltage drop across the waveguide at x=0 can now be written as

$$V^- = -\int_{z=0}^{d+h} E_z(x=0)dz = E_0 A\, e^{-jk_x c} \int_{z=0}^{d+h} \frac{f(z)}{\varepsilon(z)}\, dz \tag{4.24}$$

Substitutions for f(z) and ε(z) from equations (4.8) and (4.9) respectively into (4.24) and solving for the integral on the right side of (4.24) yields

$$V^- = E_0 A \frac{1}{\varepsilon_0}\left[\frac{d}{\varepsilon_d} + \frac{h}{\varepsilon_h}\right] = E_0 B\, e^{-jk_x c} \tag{4.25}$$

where,

$$B = \frac{A}{\varepsilon_0}\left[\frac{d}{\varepsilon_d} + \frac{h}{\varepsilon_h}\right]. \qquad (4.26)$$

This expression for B is valid for small d and h.

Using the same procedure as for V^-, the voltage drop across the waveguide at x = c can be written as

$$V^+ = -E_0 A \frac{1}{\varepsilon_0}\left[\frac{d}{\varepsilon_d} + \frac{h}{\varepsilon_h}\right] = -E_0 B. \qquad (4.27)$$

Equations (4.25) and (4.27) give the voltage drops across the waveguide at x = 0 and x = c. The next step is to examine the problem from a circuit point of view and devise a model of the overlap region.

4.3 Equivalent Circuit

The electric fields and the voltages at x = 0 and x = c are found by viewing the patch on the overlap as a rectangular planar waveguide surrounded by the electric walls on the top and bottom surfaces and the magnetic walls along the two peripheral sides of the patch. As mentioned earlier in the transmission line model, the microstrip patch can be viewed as a wide microstrip transmission line. Considering now the patch as a transmission line of the same characteristic impedance as that of the patch, the line voltages at x = 0 and x = c at the two ends of the overlap are given by equations (4.25) and (4.27) respectively. The discontinuity of the line voltage, ΔV can be written as

$$\Delta V = V^- - V^+ = E_0 B \{1 + e^{-jk_x c}\}. \qquad (4.28)$$

The line currents at x = 0 and x = c can be written as

$$I^- = -\frac{V^-}{Z_0} = -V^- Y_0, \tag{4.29}$$

and,

$$I^+ = \frac{V^+}{Z_0} = V^+ Y_0, \tag{4.30}$$

where, Z_0 is the characteristic impedance of the transmission line equivalent of the microstrip patch of width b and given by equation (2.15) and $Y_0 = 1/Z_0$.

Since the line voltage and the line current are discontinuous, the feed-patch transition (overlap) can be viewed as a π-network [23] as shown in figure-4.3. The voltage discontinuity in the equivalent transmission line of the microstrip planar waveguide is illustrated as a voltage generator connected in series with a linear circuit element. The current discontinuity introduces a π-network where the lump reactive elements represent the net reactive energy stored in the overlap region.

The primary feed line voltage and the secondary patch line voltage are not the same in general. A transformation effect should be introduced to account for the feedline and patch transition (see figure-4.3).

In figure-4.3 the ideal transformer provides a means for adjusting the coupling between the feedline source and the patch radiator so that the same amount of power is transformed from the feed source to the patch radiator that it radiates.

The remaining task is to determine the unknown circuit parameters of figure-4.3 and to develop an equivalent circuit model of the total structure by incorporating the radiation loss.

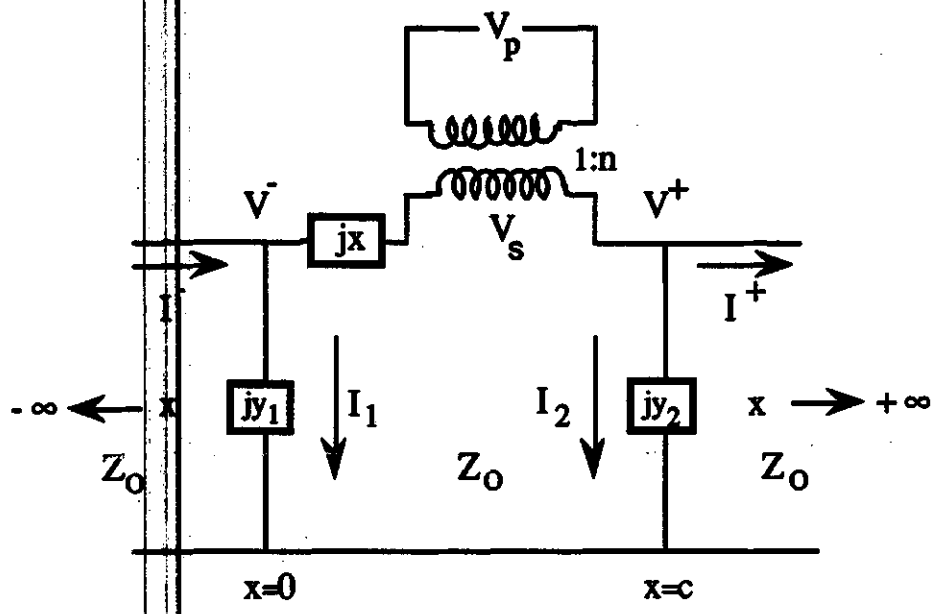

Figure-4.3 Circuit representation of the feed-patch overlap region

4.3.1 Determination of Circuit Parameters

For the equivalent circuit shown in figure-4.3 of an infinitely long transmission line of characteristic impedance Z_0, the open circuit currents are given in (4.29) and (4.30). The other currents in the circuit can be written as

$$I_1 = j V^- y_1, \tag{4.31}$$

and,

$$I_2 = jV^+ y_2, \tag{4.32}$$

where, y_1 and y_2 are to be found.

Applying Kirchhoff's current law at node x=c yields

$$I^+ + I_2 = I^- - I_1,$$

substituting for I_1 and I_2 from (4.31) and (4.32) respectively and rearranging the above equation yields

$$I^+ - I^- = -(I_1 + I_2) = -j[V^- y_1 + V^+ y_2] \tag{4.33}$$

Substituting for the values of V^-, V^+, I^-, I^+ from equations (4.25), (4.27), (4.29), (4.30) into equation (4.33) and equating the real and imaginary parts separately, yields

$$y_1 = y_o \frac{1 - \cos(k_x c)}{\sin(k_x c)}, \tag{4.34}$$

$$y_2 = -y_o \frac{1 - \cos(k_x c)}{\sin(k_x c)} = -y_1. \tag{4.35}$$

By using Kirchhoff's voltage law across the source between x=0 and x=c yields

$$V^- - V^+ = (I^+ + I_2)jx + nV_p \tag{4.36}$$

where, V_p is the primary source voltage between the feed line and the ground plane. Substituting for the values of V^-, V^+, I^-, I^+ from equations (4.25), (4.27), (4.29) and (4.30) into equation (4.36) and equating the real and imaginary parts separately as before, x and n can be written as

$$x = Z_0 \sin(k_x c), \tag{4.37}$$

$$n = 2B\frac{E_0}{Vp} = 2\frac{B}{d}, \tag{4.38}$$

where, the primary feed line voltage Vp at x=0 is dE_0.

Equations (4.34), (4.35), (4.37) and (4.38) are the required expressions for the circuit parameters of the feed-patch transition. The parameters y_1, y_2, x and n are functions of feed inset c, substrate dielectric constants ε_d and ε_h, substrate thickness d and h, feed line width w, patch dimension b, and operating frequency.

4.3.2 Input Impedance

The complete equivalent circuit of the EMC microstrip patch antenna is obtained from figure-4.3 by simply adding the effect of the radiating slots at its two ends. Instead of the open circuit the slots are viewed as the radiation admittances Y_r connected at both ends. The radiation admittance Y_r is given in equation (2.18). This means that figure-4.3 can be modified as shown in figure-4.4. Figure-4.4 illustrates the complete equivalent circuit model of an EMC microstrip patch antenna.

The patch has two radiation slots at x=0 and x=a. Since one radiation edge is at x=0, the radiation admittance Y_r is directly connected to the terminals at x = 0. For the other radiation edge at x= a, the second radiation admittance Y_r is connected through a transmission line of length (a-c). The line has the same characteristic impedance Z_0 and propagation constant k_x as those of the microstrip patch.

From the complete equivalent circuit model as illustrated in figure-4.4, the input impedance of the EMC microstrip patch antenna is obtained by transforming the radiation admittance Y_r through the low impedance microstrip line of characteristic impedance Z_0 given in (2.15). In the figure Z_1 and Z_2 are the input impedances seen by the secondary source V_s at x = 0 and x=c respectively. Z_1 and Z_2 can be written as

$$Z_1 = jx + \frac{1}{Y_r + jy_1}, \tag{4.39}$$

$$Z_2 = jy_2 + Y_0\frac{Y_r + jY_0\tan\{k_x(a-c)\}}{Y_0 + jY_r\tan\{k_x(a-c)\}}^{-1}, \tag{4.40}$$

where, $Y_0 = 1/Z_0$, the characteristic admittance of the patch antenna.

The input impedance of the antenna with respect to the primary feed point at x = 0 can be written as

$$Z_{in} = \frac{(Z_1 + Z_2)}{n^2}, \tag{4.41}$$

where, n is the turns ratio of the ideal transformer given in (4.38).

Equation (4.41) is the input impedance formula of an EMC rectangular patch antenna on a two-layer substrate. By using the formula a computer program is written to compute the input impedance. From the input impedance data other characteristic parameters such as return loss, resonant frequency and bandwidth are determined. The numerical results will be presented in the chapter that follows.

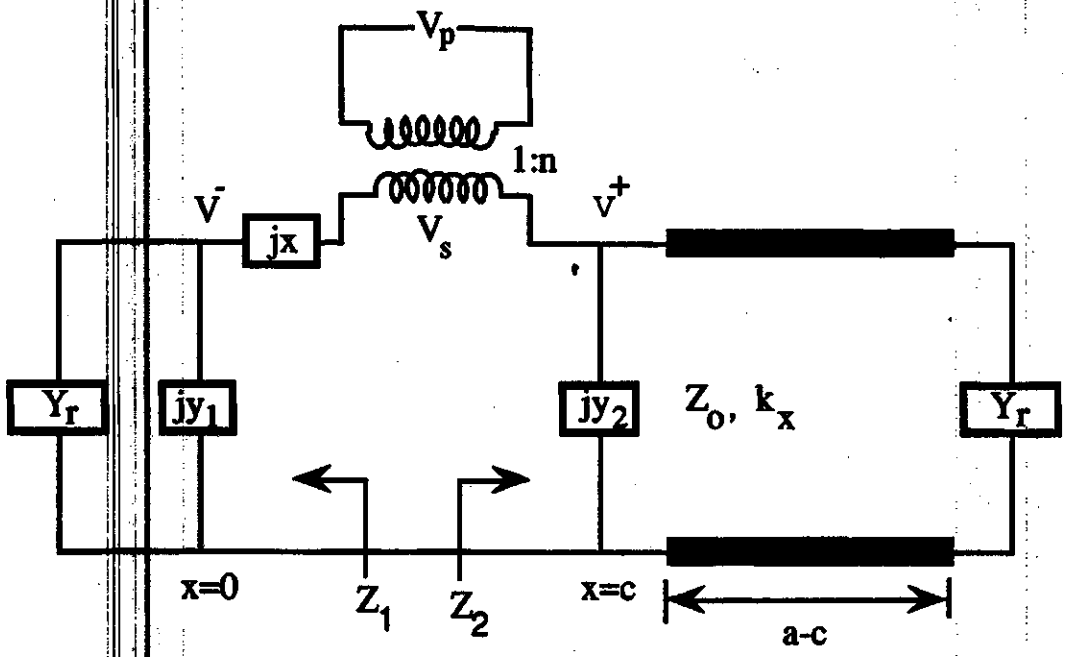

Figure-4.4 Equivalent circuit of an EMC microstrip patch antenna

4.4 Conclusion

A simple equivalent circuit model of a two-layer electromagnetically coupled rectangular microstrip patch antenna has been developed. In the development of the circuit model the analysis was two-fold. First, the feed-patch transition model was developed and next the radiation effect of the patch radiator was incorporated. In the development of the transition model, the unknown fields in the overlap were determined by invoking the reciprocity theorem. By using the electric field thus determined, the secondary line voltages and circuit parameters were found. The complete equivalent circuit model was obtained by adding the radiation admittances at the radiating edges. From the complete equivalent circuit, the input impedance seen by the feed line was derived. The input impedance of the EMC patch antenna was obtained by the simple formulae (4.34), (4.35),

(4.37), (4.38), (4.39) - (4.41). This simple expression of the input impedance reveals the simplicity of the model.

Comparing the circuit model developed in the present method with that of the transmission line model in chapter two, it is observed that the present model contains more lump reactive elements. This yields more accurate representation of the net reactive energy stored in the overlap region. The method is more generalized because it can be applied to higher order modes.

The following chapter will discuss the results obtained by utilizing different approaches presented in preceding chapters.

5. RESULTS AND DISCUSSIONS

5.1 Introduction

In this chapter a comparison of the theoretically predicted results is made by using various methods described in the previous chapters with respect to the experimental data. Such a comparison will give a measure of confidence in the analytical methods undertaken in this thesis. Different performance characteristics of an EMC patch antenna in terms of the design parameters are also discussed.

The following sections will deal with the experimental and theoretical results obtained for an EMC rectangular patch antenna composed of two dissimilar substrates. The frequency range used was from 3.5 Ghz to 4.5 Ghz. The choice of dissimilar substrates offers a flexible design performance as well as removes the difficulty of coupling between the feed circuitry and the radiator elements (see chapter-1). The input impedance curves will provide with the estimates of the design parameters, namely the resonant input resistance, resonant frequency and the bandwidth. Comparison of theoretical and experimental input impedance curves will prove the validity of the theoretical methods.

The theoretical results and the experimental data will be compared with respect to the return loss and input impedance of the antenna. The experimental data were recorded for various frequencies by using the

HP8510B network analyzer. The experimental procedures will be presented in the appendix.

5.2 Comparison of Theoretical and Experimental Results

The input impedances of the EMC patch antenna were computed numerically by using equations (2.32), (3.55) - (3.56) and (4.39) - (4.41). The corresponding return losses were found from the numerical input impedance data by using the formula

$$RL_{in}\,dB = 20 \log_{10} \left| \frac{Z_{in} - Z_f}{Z_{in} + Z_f} \right|, \qquad (5.1)$$

where, Z_{in} is the input impedance obtained numerically from equations (2.32), (3.55) - (3.56) and (4.39) - (4.41) and Z_f is the characteristic impedance of the feed line. The feed line was designed for a characteristic impedance of 50Ω (Z_f = 50Ω) using the design formulae given in [32].

The numerical results will be compared to the experimental results by illustrating different plots of the data. In the following sections the plots will be shown in different graphs followed by a discussion on the results obtained.

5.2.1 Return Loss

The return loss curves were produced in figure-5.1 for a patch of length a=2.22cm and width b=2.00cm by using data obtained from the theoretical analyses and experimental results. The other specifications of the EMC patch antenna in the measurements were: the lower substrate

was a DICLAD-870 of dielectric constant ε_d = 2.33±0.04, and thickness d = 0.0794cm, the upper substrate was a TLY-5 of dielectric constant ε_h = 2.22±0.02 and thickness h = 0.15874cm. The length of the feed line L = 7.62cm of which a feed inset c = 1.11cm [(c/a)×100% = 50% overlap]. The width of the feed line was (w) 0.2413cm. The specifications given above will remain the same throughout the following comparisons except the patch width b and length a. In all the numerical computations ε_d and ε_h were considered to be 2.33 and 2.2 respectively though the uncertainty of the exact values still remains.

Return loss of an antenna is a measure of degree of match between the radiator element and feed network [see equation (5.1)]. The higher the return loss, the better matched are the patch and the feed network. Maximum return loss in a given frequency range occurs near the resonant frequency of the antenna. This is not an unreasonable approximation to consider the frequency of maximum return loss to be the resonant frequency of the antenna. Thus from return loss curve two important parameters of the antenna can be predicted, namely the degree of match and the resonant frequency.

In figure-5.1 the return loss curves were obtained from the plots of the measured return loss data and the calculated return loss data from the three different approaches, using the same parameters. Thus the curve consists of four different plots. By comparing the theoretical results to the experimental results one can immediately see that there is some similarity in the shapes of the curves as well as some significant differences. Obviously the more closely related curves to the experimental one the better the theory explains the reality.

From figure-5.1 the maximum return loss obtained from the experimental data was -17.61dB at 4.10 Ghz. Those obtained from the theories, namely transmission line model, cavity model method and planar

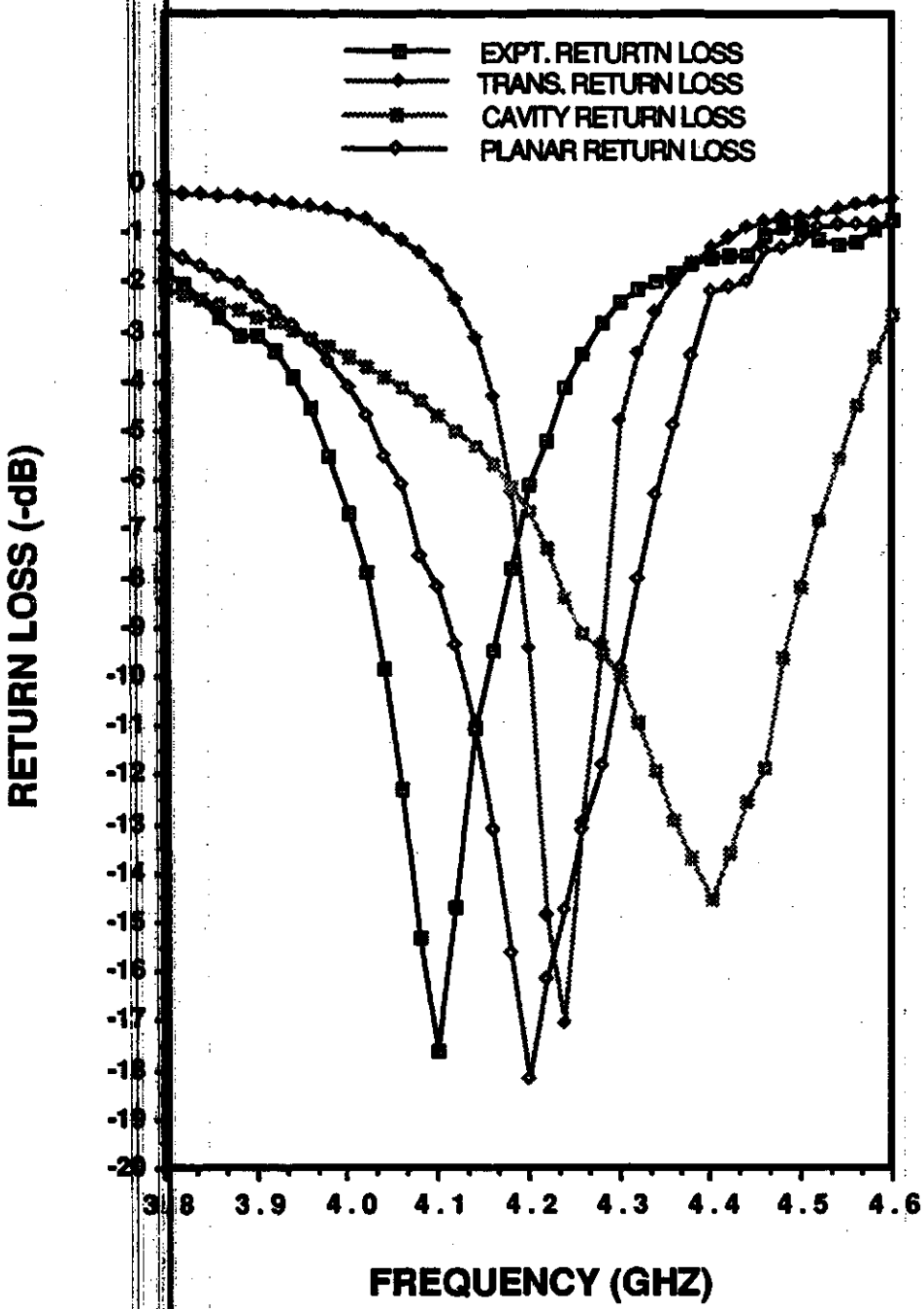

Figure-5.1 Return loss curve

waveguide theory were -17.03dB at 4.24Ghz, -14.52dB at 4.40Ghz and -18.21dB at 4.20Ghz respectively. The departures of the maximum return losses of the theories from that of the experimental results were 3.35% less, 17.65% less and 3.4% higher for transmission line model, cavity modal method and excitation of waveguide method respectively. The theoretical resonant frequency shifts from that of the experiment were 3.41% upward, 7.3% upward, and 2.44% upward respectively. By comparing the theoretical and experimental results one can immediately see that the curve obtained from the planar waveguide method is the closest to the curve obtained from the experimental plots.

The half power bandwidth obtained from the theoretical analyses can be compared to that determined from the experimental data. Usually -10dB return loss bandwidth is called the bandwidth of the antenna [25]. In figure-5.1 the -3dB bandwidths are 2.7%, 2.0%, 3.9% and 3.4% from the experimental results, transmission line model, cavity modal method, and planar waveguide method respectively. The theoretical bandwidth discrepancies from that of the experimental results were 1.3% less, 1.2% greater and 0.7% greater for the three theories in order. The bandwidth performance is the best for planar waveguide method.

The comparison of the theoretical and the experimental return losses was conducted for four different EMC microstrip patches. The patch widths were 1.00cm, 2.00cm, 3.00cm and 4.00cm respectively. For each patch the length of the patch was 2.22cm and the feed inset was half the patch length (1.11cm). Table-1 shows the comparison of the maximum return losses and the corresponding frequencies obtained from the experimental data and the theoretical results. Table-1 shows that in the experimental results the resonant frequencies decrease gradually with EMC patch width. For this

particular feed inset the maximum return loss obtained was -17.6dB for a patch of width 2.00cm and the minimum return loss obtained was -6.88dB for a patch of width 4.00cm. The results obtained from the transmission line model analysis shows higher resonant frequencies departures than those of the experimental results and for wider patches the maximum return loss deviates largely (about 50% less than the practical return loss). Cavity modal analysis produced results almost invariant resonant frequencies (around 4.42Ghz) and maximum return loss (-10.0dB). There are some remarks on this theory that are mentioned in the conclusion. The planar waveguide analysis produced results closest to the experimental results with respect to both the maximum return loss and resonant frequency for all the four patches.

TABLE - 1

COMPARISON OF MAXIMUM RETURN LOSSES AND CORRESPONDING FREQUENCIES FOR FOUR EMC RECTANGULAR MICROSTRIP PATCHES

(PATCH LENGTH = 2.22cm, FEED INSET = 1.11cm)

PATCH WIDTH (cm)	EXPERIMENT		TRANS. LINE MODEL		CAV. MODAL ANALYSIS		PLANAR WAVE-GUIDE	
	FREQ. (Ghz)	RL_{max} (-dB)	FREQ. (Ghz)	RL_{max} (-dB)	FREQ. (Ghz)	RL_{max} (-dB)	FREQ. (Ghz)	RL_{max} (-dB)
1.00	4.2	-12.7	4.27	-15.8	4.43	-12.8	4.27	-10.5
2.00	4.1	-17.6	4.25	-16.5	4.40	-15.7	4.20	-18.2
3.00	4.0	-10.5	4.20	-5.72	4.42	-10.1	4.14	-9.29
4.00	4.0	-6.88	4.17	-3.31	4.43	-11.0	4.07	-6.16

Finally, from the comparison of the theoretical results to the experimental results with respect to the maximum return loss, resonant frequency and bandwidth it can be concluded that the planar waveguide theory explains the reality best.

Although the differences between results obtained from the theoretical analyses and the experimental data are much high, the theoretical results still provide reasonable estimation. The resonant frequency shifts and return loss departures from the reality can be attributed to the fabrication tolerance and the uncertainty of the dielectric constants [1].

5.2.2 Input Impedance;

In the preceding section comparisons between the theoretical and the experimental results have been made with respect to antenna return loss, and some parameters of an EMC patch antenna namely, the maximum return loss, resonant frequency and bandwidth were predicted. However, the comparisons based on return losses were indirect [see equation (5.1)]. In this section the quantitative (direct) comparison between the theoretical and experiment results will be conducted with respect to the input impedance of the antenna and some other parameters will be predicted.

Input impedance of an antenna is defined as the impedance presented by an antenna at its terminals or the ratio of voltage to current at a pair of terminals or the ratio of the appropriate components of the electric to the magnetic fields at a point. The input impedance is generally a function of frequency. For a lossless antenna (losses other than radiation loss), the real part of the input impedance is called the input resistance or

the radiation resistance of the antenna and the imaginary part is called the input reactance of the antenna. The input impedance of the antenna should be conjugate matched to the impedance of the feed circuit to maximize the power delivered to the antenna [18]. Thus the input impedance of an antenna is a very important parameter and it can be used to determine antenna efficiency. The followings are the comparisons of the input impedances obtained from the theoretical results and the experimental data.

(a) Transmission line model input impedance

Figure-5.1 illustrates the plots of input impedance data obtained from the experimental results and the results obtained from the transmission line model analysis for a patch of length 2.22cm and width 1.00cm at 50%overlap using the same parameters.

As can be seen from the plots each of the curves crosses the zero input impedance axis when the input resistance is maximum. The intersections are points at which resonance occurs (i.e. the inductive and capacitive reactances cancel; the impedance is a real quantity). The input resistance at the resonance is called the resonant input impedance (resistance) and the corresponding frequency is called the resonant frequency. The resonant input resistances were 106.23Ω and 84.83Ω from the experimental plots and the transmission line model plots respectively. The corresponding resonant frequencies were 4.21Ghz and 4.19Ghz respectively. The half power bandwidth obtained from the experimental and the theoretical results were 2.14% and 4.5% respectively. The theory yields 20% less resonant input resistance, 0.5% downward resonant frequency shifts and 2.3% larger

bandwidth. Despite these discrepancies the theoretical results still provide the reasonable estimation of resonant input resistance.

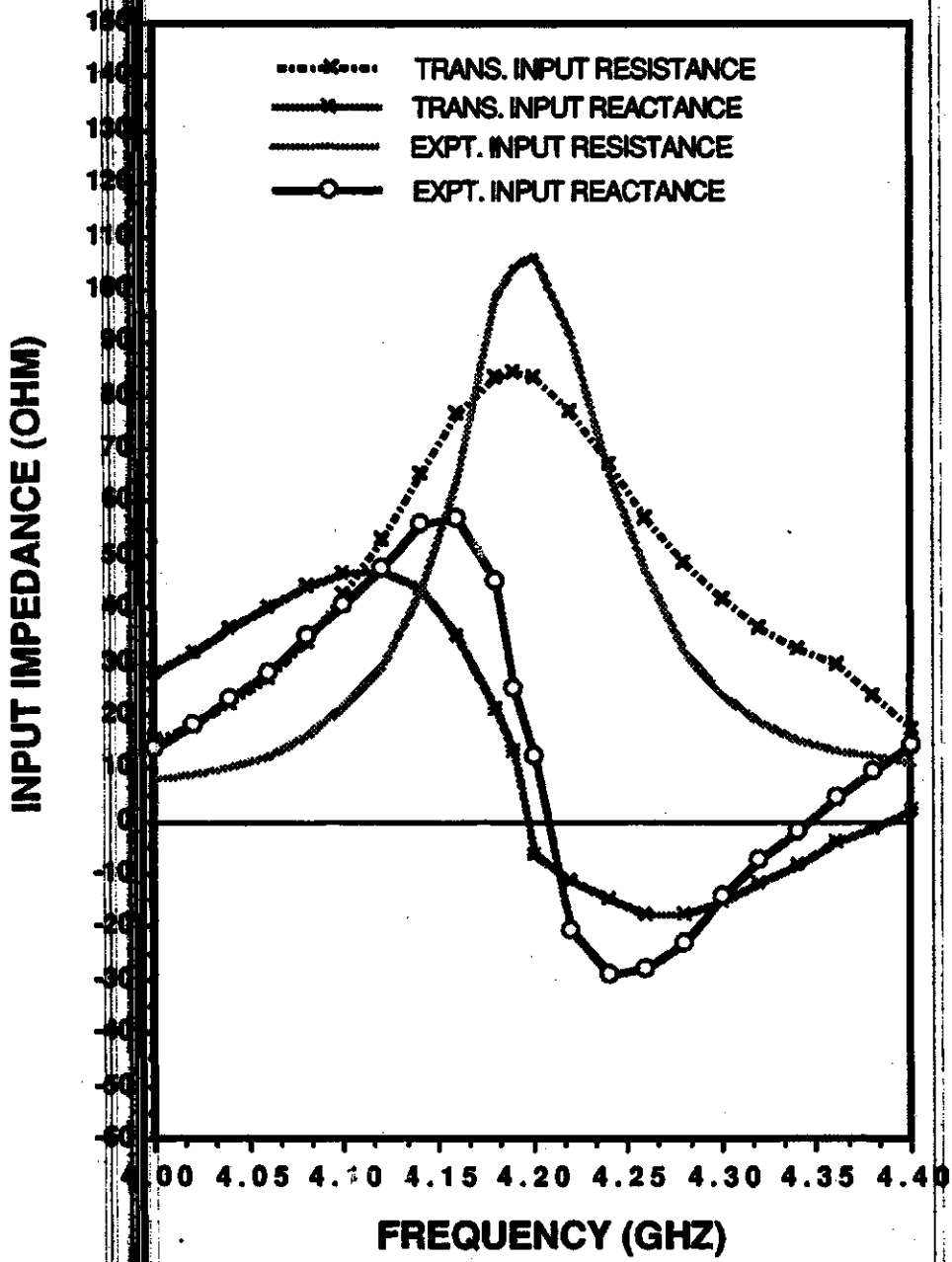

Figure-5.2 Transmission line model input impedance curve

(b) Cavity modal analysis input impedance

In figure-5.3 input impedance curves were produced from the data obtained from the cavity modal analysis and the data obtained from the measurements for a patch of length 2.22cm and width 1.0cm at 50% overlap, using the same measurement specifications as before. The resonant input resistance obtained from the theoretical analysis was 113.11Ω at a resonant frequency of 4.16Ghz. Those determined from the measured data were 106.23 Ω at 4.21Ghz. The half power bandwidth obtained from the analytical results was 5.77% and the same determined from the experimental results was 2.14%. From the plots it can be seen that the analytical results using cavity modal method produced a higher bandwidth than that of the experimental results by a factor of 3.63%. The resonant resistance estimated from this method were 9% greater than that of the experimental results and resonant frequency shifts upward from the experimental resonant frequency by a factor of 1.2%. From the comparison it can be concluded that though the resonant frequency shift and bandwidth discrepancy from those of the experimental results are high, the input impedance estimate is quite reasonable.

(c) Planar waveguide model input impedance

Figure-5.4 illustrates the plots of input impedance data obtained from the analysis of excitation of waveguide method and that determined from the measured data for a patch of length 2.22cm and width 1.00cm at 50% overlap, using the same measurement specifications. By comparing the theoretical results to the experimental results one can immediately see that there is a uniform agreement between these two different plots though the

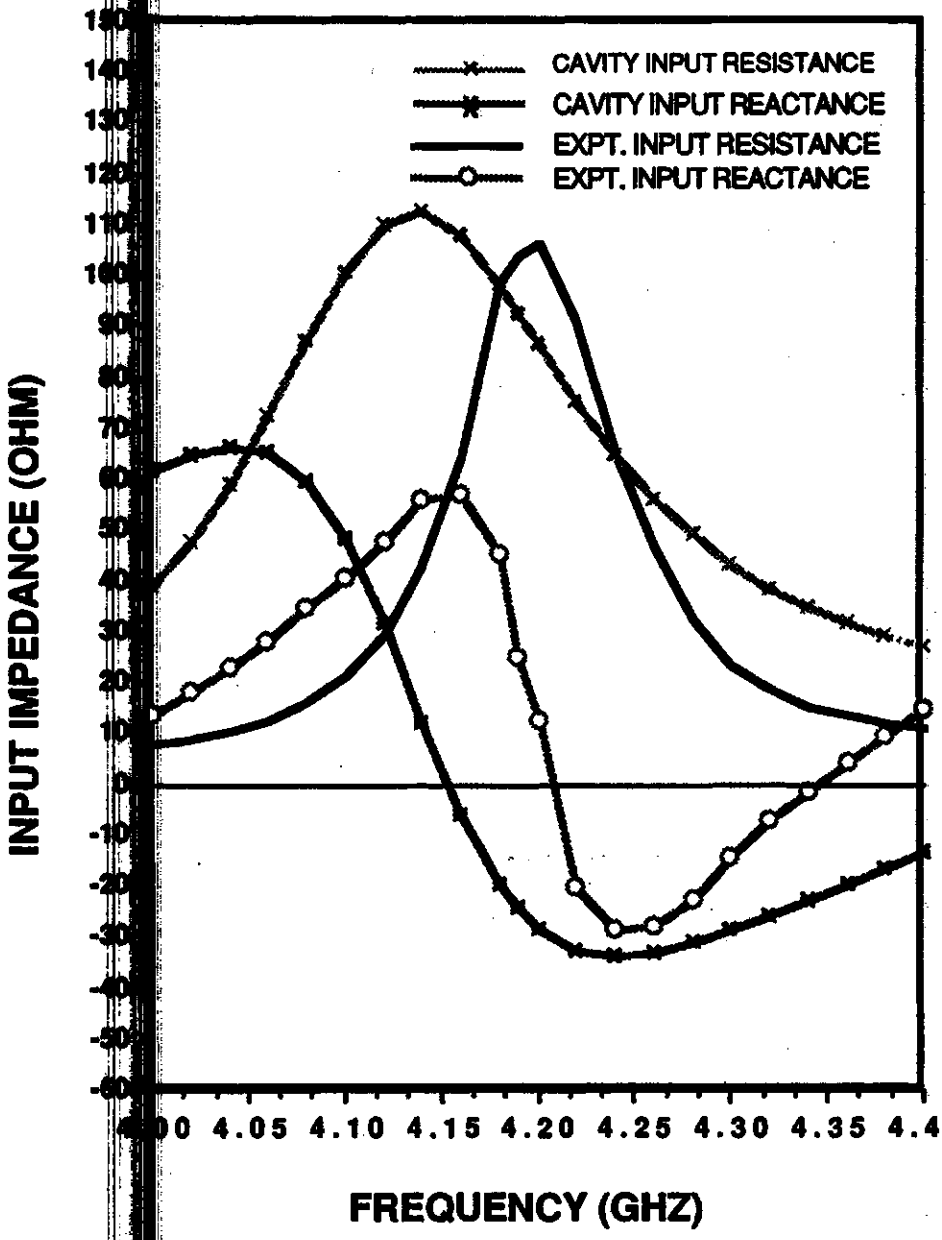

Figure 5.3 Cavity modal theory input impedance curve

theory shows a higher input impedance values by a factor of about 7%. The resonant input resistance obtained from the theoretical results and the measured data were 124.78Ω and 106.23Ω respectively. The corresponding resonant frequencies were 4.20Ghz and 4.21Ghz respectively. The -3dB

bandwidth obtained from the theoretical results and the experimental results were 4% and 2.14% respectively. The theoretical estimations show that the resonant resistance, resonant frequency and the bandwidth discrepancies from those of the experimental results were 12% greater, 0.3% upward shift and 1.86% larger respectively.

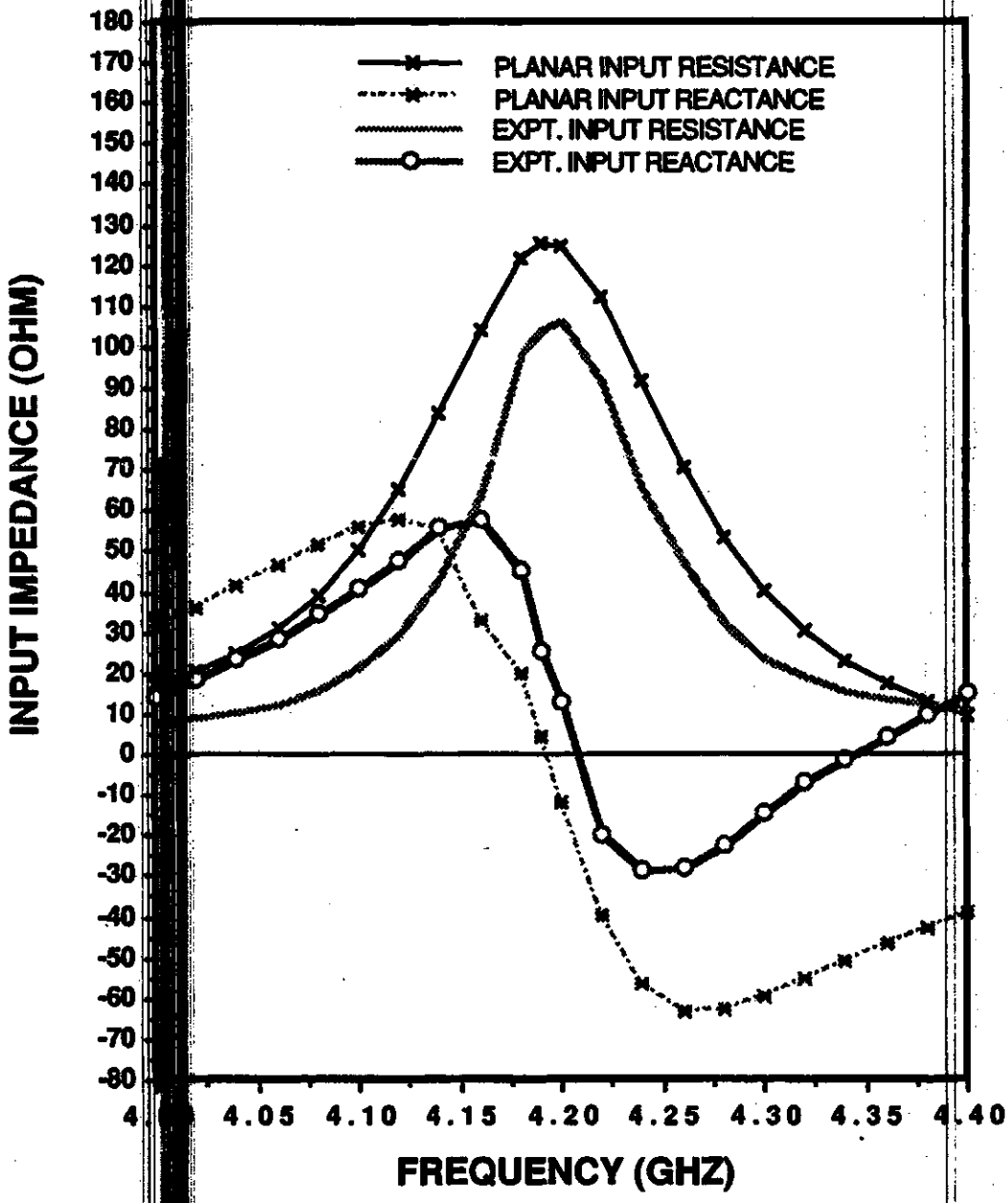

Figure 5.4 Planar waveguide model input impedance curve

Finally, comparison of the three sets of input impedance plots shows that the theoretically predicted resonant resistances and resonant frequencies were always larger than those determined from the measured data. However, the discrepancies are within reasonable tolerance (highest 20% resonant resistance and 1.2% resonant frequency). Obviously the most closely curve to the experimental plots is obtained form the excitation of waveguide method. Thus it can be concluded that this method explains the observations best.

In this section comparisons between the results obtained from the theoretical approaches and the results determined from the experimental data were conducted based on the return loss and input impedance. Comparison based on return loss provides with a qualitative picture and predicts some important characteristics of the antenna. Using results based on the input impedance data, quantitative comparisons were made. The important antenna parameters, namely return loss, resonant input resistance and resonant frequency were investigated with respect to the patch dimensions. The agreement between the theories and the experiments were in general good. Comparison shows that the results obtained from the planar waveguide theory were in the best agreement of the three approaches undertaken in this thesis with respect to the experimental results. It is appropriate to conduct theoretical design procedure based on the results obtained from the planar waveguide theory.

5.3 Theoretical Design Curves

The important design parameters of the microstrip patch antenna are resonant input resistance, resonant frequency, patch width and patch length. The patch length of the rectangular microstrip antennas is usually

half the resonant wavelength of the antenna [1]. The designed value of the patch length is directly related to the resonant frequency of the antenna. The patch width is inversely proportional to the input resistance (radiation resistance) of the antenna (see equation 2.11). The wider the patch the less the radiation resistance of the antenna. The followings are the theoretical plots of design parameters obtained from the planar waveguide theory for the two-layered EMC microstrip patch antenna.

(a) Input resistance at resonance vs patch width

In figure-5.5 resonant input resistance curve was produced against patch width for various patches. The patch length was considered to be 2.00cm and the feed inset was half the patch length. The other measurement specifications were the same as before. From the curve it can be seen that the resonant input resistance of the EMC patches is a monotonic increasing function of the patch width provided that the other physical dimensions of the antenna remain the same. The inverse proportionality of the resonant input resistance to the patch width agrees with the equation (2.11). From the curve the optimum patch width required for a desired resonant input impedance match can be found. For example, for a 50Ω input impedance at resonance, the design value of the EMC patch length obtained from the plots was 1.59cm. Thus this curve provides with the estimates of the important design parameters, namely the resonant input impedance and the corresponding patch width of an EMC patch antenna.

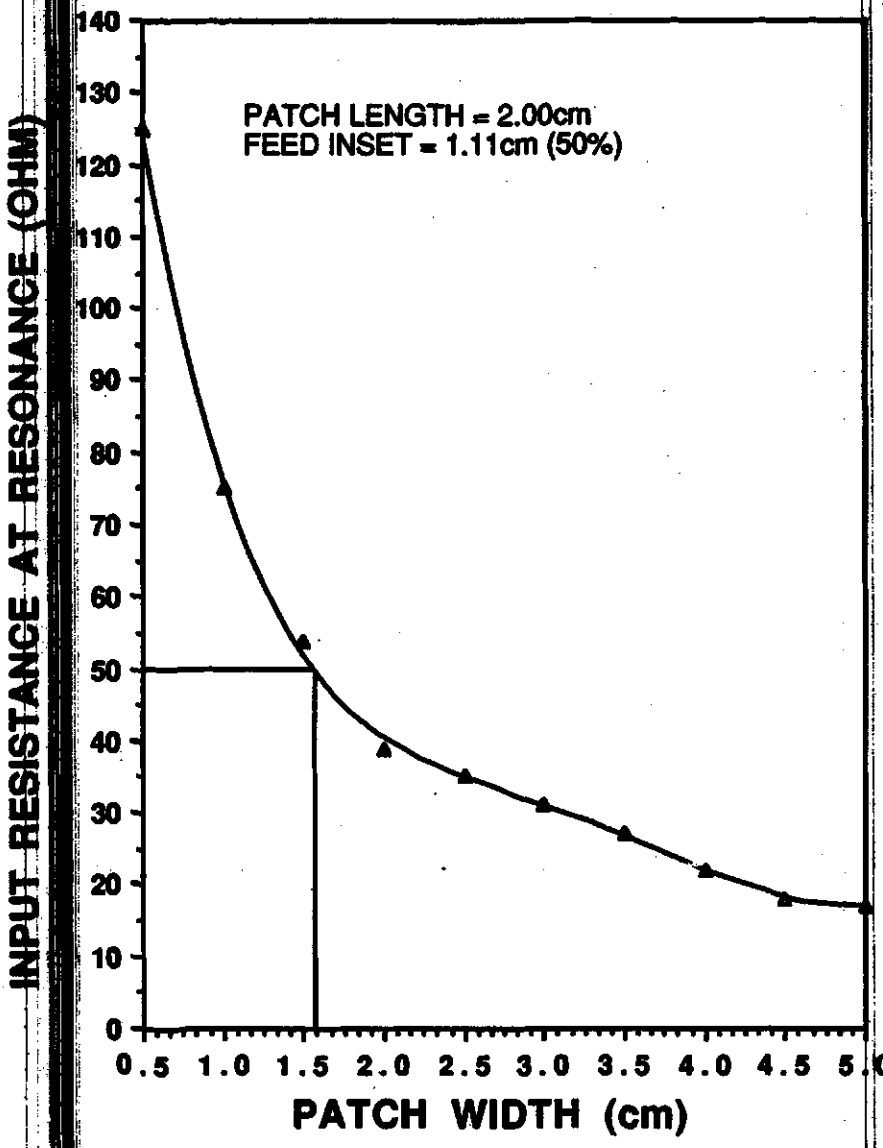

Figure-5.5 Input resistance at resonance vs patch width

(b) Resonant frequency vs patch length

The resonant frequency curve was produced against the patch length using input impedance data obtained from the planar waveguide theory. Figure-5.6 illustrates the variation of the resonant frequency with the variation of the patch length for various patches. The patch width was

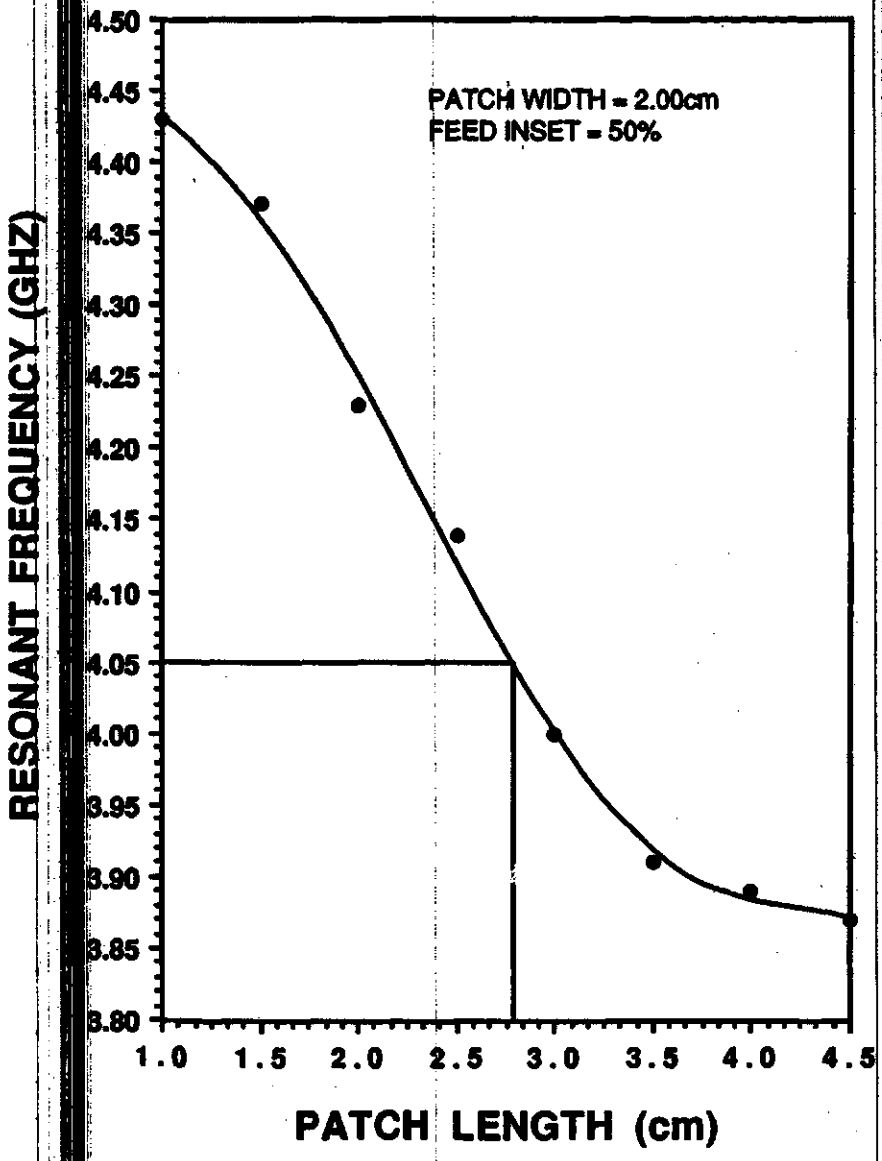

Figure-5.6 Resonant frequency vs patch length

considered to be 2.00cm and the feed inset was always half the patch length. The other measurement specifications were the same as before. It can be seen from the curve that, the resonant frequency decreases with the patch length as expected provided that the other physical parameters of the antennas were fixed. From the curve important design information of the

patch length and the resonant frequency can be extracted. For example, for a EMC patch antenna operating at 4.05Ghz resonant frequency, the theoretically obtained designed value of the patch length was 2.82cm. The information can be used in the practical EMC antenna design.

5.4 Conclusion

In this chapter comparisons between the results determined from the experimental data and the results obtained from the theoretical approaches were conducted based on the return loss and input impedance. Comparisons based on return loss gave merely a qualitative picture and predict some important characteristics of the antenna. Using results based on the input impedance data the quantitative comparisons were made. The important design parameters of the antenna, namely the resonant input resistance, the resonant frequency and bandwidth were investigated with respect to the return loss and input impedance of the EMC patch antenna. The agreement between the theoretical results and the experimental results were in general good. In the analytical approaches the planar waveguide method produced the results most closely to the experimental results. The theoretical design plots were presented from the results obtained by using planar waveguide method. The discrepancies in resonant frequencies and input impedances can be attributed to the fabrication tolerance and uncertainty of the substrate dielectric constants [1].

6. CONCLUSIONS

Electromagnetic coupling is found to be a very promising feed technique that could be used in the production of linear antenna array [15]. Higher bandwidth and gain, ease of fabrication, reduced spurious radiation from the feed network make the EMC patch antenna an attractive topic of antenna research. This method provides for flexibility in choosing the substrates which best meet the conflicting requirements of the total structure (namely high dielectric constant for the feed and low dielectric constant for the antenna elements). In addition, the fact that the lower substrate is very close to the ground plane is very useful since this will provide least feed radiation distortion. The choice of thicker upper substrate increases the bandwidth [7] where lower bandwidth is an inherent problem to the microstrip patch antenna.

The interest in electromagnetic coupling has been growing steadily as more researchers become involved in the problem of *narrow bandwidth* and *construction complexity*. The work presented in this thesis is both mathematically simple and practically efficient. The work includes both the theoretical analyses of the problem in three different approaches and their experimental verification.

The objectives of this thesis were to analyze the EMC patch antenna with different theoretical methods, to develop an appropriate analytical method that can predict accurately the characteristics of an EMC patch

antenna, to verify and compare the analytical approaches with the experimental results, and finally, to develop the design procedures for the EMC patch antenna using the appropriate method. To satisfy the first objective of this thesis, the theoretical analysis was started with the transmission line model. The patch was viewed as a transmission line loaded by the radiation impedances at both ends. The feed patch transition was represented by an ideal transformer connected in series with the transmission line. Modal field expansion of the feed line field was used to derive the turns ratio of the ideal transformer. By combining the transformation effect to the transmission line equivalent of the patch, the circuit model of the EMC patch antenna was developed. From the circuit model the input impedance of the EMC patch antenna, as seen by the feed line at its end, was formulated. The input impedance formula was computer programmed to produce the theoretical input impedance data. From the theoretical data the resonant frequency, resonant input resistance and bandwidth for a given feed inset and patch dimensions were determined.

The cavity model of a patch element was presented in chapter-3. Modal expansion of the cavity fields was carried out on the model so that the fields could be found. The wave equation of the feed line source was produced as the governing equation that predicted which mode fields would be excited inside the cavity. The dominant mode in the cavity was considered to be the TM_{10} mode and fields calculations were limited to the dominant mode only. From the field solution the radiation power and the stored power of the patch antenna were obtained. The total power delivered by the feed line is considered to be the summation of these two powers. From the total power it was possible to obtain an expression for the input

impedance seen by the feed line at its end. The theoretical input impedance data were produced using the input impedance formula.

In the development of the accurate analytical method planar waveguide method was proposed for an EMC patch antenna [31]. This met the second objective of this thesis. In this method, the EMC patch antenna was considered to be a planar waveguide in which a microstrip feed was inserted laterally, supporting TEM wave modes. The electric fields inside the waveguide was found by using the reciprocity principle. From the fields the voltage drops across the waveguide and the line currents were determined. Both the voltages and currents were discontinuous across the source. Due to the discontinuities of both the voltage and current a π-circuit model for the source was developed. By incorporating the radiation effect of the patch with the transition circuit, the complete equivalent circuit was developed. Input impedance formula was obtained from the equivalent circuit. The formula was used to collect numerical design data.

Objective three was met by a check on the validity of the analytical approaches and a comparison between them. Theoretical data points were produced by using the same parameters as those of the experimental measurements. The experiments were conducted by using the HP 8510B vector network analyzer. To gain confidence on the theoretical methods as well as predict different parameters of an EMC patch antenna, comparisons were made with respect to return loss, input impedance, resonant input impedance, resonant frequency and bandwidth. Comparisons showed reasonable agreement between the theoretical and experimental results as well as some significant differences. The discrepancies of the theoretical parameters from the experimental parameters were also considered to be within the tolerable limits. It was

therefore concluded that the theoretical development as well as the computer program generating data points provides reasonable estimates of resonant frequency and resonant input resistance. These discrepancies of the resonant resistance and resonant frequency can probably be attributed to the fabrication tolerance and uncertainty in the values of the substrate dielectric constants.

In the comparison the input impedance plots produced by the transmission line model data showed the resonant frequency distortion by a factor of 0.5% downward shift from that of the experimental results. The other discrepancies were 20% less resonant input resistance and 2.2% larger bandwidth than those of the experimental results. These discrepancies can be attributed to the simplest design formula of input impedance derived in the approach. Moreover, to keep the mathematics simple as possible mutual coupling between the radiation slots, losses due to the dielectric materials, conductor were not considered in the theoretical analyses. Thus it was expected that there would be some differences between the theoretical and experimental results.

The cavity modal method for the EMC rectangular patch antenna was analyzed for the TM_{10} dominant only. Usually in this particular mode the patch length was considered to be greater than the patch width. In this mode the radiation loss is due to the two radiating edges spaced half-wavelength apart. The results obtained from the input impedance computation for a patch of length 2.22cm and width 1.00cm showed estimates of 9% greater resonant input resistance, 1.2% downward shift in resonant frequency and 2.66% larger bandwidth than those of the experimental results. This results were in good agreement with the experimental results. For patches of width larger than the patch length,

this modal calculation does not couple with the experimental results as the input impedance is directly proportional to the patch dimensions [see equations (2.55) and (2.56)].. Thus for the analytical results based on the particular dominant mode, the discrepancies from the experimental results are not unexpected. Like transmission line model analysis, the mutual coupling of the radiating edges was not considered in this analysis. To obtain results closely to the experimental results, it is necessary to consider other modes in the cavity.

Finally, objective four was satisfied with the simple method that was proposed to analyze the EMC patch and develop the design procedures. The planar waveguide method produced the results most closely to the theoretically predicted results. The prediction of both the resonant frequency and the resonant input resistance were in good estimations of the experimental predictions. The analysis produced results with a uniform agreement with respect to both the return loss and input impedance. The results obtained from the analysis were 12.0% higher resonant input resistance, 0.3% upward shift of the resonant frequency and 1.86% larger bandwidth than those of the experimental results. From the work done to this point it is reasonable to conclude that the less theoretically rigorous analysis does produce good estimates for the input impedance of an EMC patch antenna. The input impedance curves produced from the plots of input impedance data have yielded good results when compared to the experimentally derived curves. So, in the region from 3.5 to 4.5Ghz the analysis of chapter four produces good results. As anticipated, the discrepancy between the theoretical and the experimental values are very close. Theoretical design curves were presented using the results obtained from the planar waveguide theory.

REFERENCES

[1] I.J. Bahl and P. Bhartia, *Microstrip Antennas*, Dedham, MA:Artech House, 1980.

[2] W.F. Richards, "Microstrip antennas", *Antenna Handbook: Theory, Applications, and Design*, New York: Van Nostrand Reinhold Co., 1988.

[3] R.K. Hoffmann, *Handbook of Microwave Integrated Circuit*, Dedham, MA: Artech House, 1987.

[4] J.A. Navarro, K.A. Hummar and K. Chang, "Active integrated antenna elements", *Microwave Journal*, pp.115-126, Jan.,1991.

[5] D.H. Schaubert, R.W. Jackson, and D.M. Pozar, "Antenna elements for integrated phased arrays", *IEEE Proceedings of the 1985 Antenna Applications Symposium*, RADC-TR-85-242, Vol.- 1, Dec., 1986.

[6] J.R. James, P.S. Hall, and C.Wood, *Microstrip Antenna: Theory and Design*, Stevenage, U.K.: Peter Peregrinus Ltd., 1981.

[7] D.F. Hunter and K.C. Gupta, "Multiport network modeling of electromagnetically coupled microstrip patches", *ANTEM'90*, Winnipeg, Canada, PP.32-37,1990.

[8] R. Q. Lee, K.F. Lee, and J. Bobinchak, "Characteristics of a two-layer electromagnetically coupled rectangular patch antenna",*Electron. Lett.*, vol.23, no.15, pp.1070-1072, Sept. 1987.

[9] P.L. Sullivan and D.H. Schaubert, "Analysis of an aperture coupled microstrip antenna", *IEEE Trans. Antennas Propagat.*, vol.AP-34, pp.977-984, Aug., 1986.

[10] D.M. Pozar, "Microstrip antenna aperture-coupled to an microstripline", *Electron. Lett.*, vol.21, no.2, pp.49-50, 7th Jan., 1987.

[11] G. Split, "Rectangular electromagnetically coupled microstrip antennas in multilayered structures", *Proc. 18th European Micro. Conf.*, pp.1043-1048, 1988.

[12] R. Q. Lee, K.F. Lee,"Gain enhancement of microstrip antennas with overlaying parasitic director", *Electron. Lett.*, vol.24, no.11, pp.656-658, May, 1988.

[13] D.M. Pozar and B. Kaufman, "Increasing the bandwidth of a microstrip antenna by proximity coupling", *Electron. Lett.*, vol.23, no.11, pp.687-690, Mar., 1987.

[14] P.B. Katehi and N.G. Alexopoulos, "On the modeling of electromagnetically coupled microstrip antennas - the printed strip dipole", *IEEE Trans. Antennas Propagat.*, vol.AP-32, pp.1179-1186, Nov., 1984.

[15] D.R. Jackson and P. Manghnani, "Analysis and design of a linear array of electromagnetically coupled microstrip patches",*IEEE Trans. Antennas Propagat.*, vol.AP-38, pp.754-759, Aug., 1989.

[16] D.L. Sengupta,"Transmission line analysis of rectangular patch antennas", *Electromagnetics*, vol.4, pp.355-376, 1984.

[17] N.G. Alexopoulos, N.K. Uzunoghn and I. Rana, "Radiation by microstrip patches",*IEEE AP-S Int, Symp. Digest,* pp.722-772, 1979.

[18] C.A. Balanis, *Antenna Theory: Analysis and Design*, New York: John Wiley & Sons, 1982.

[19] W.L. Weeks, *Antenna Engineering*, New York:McGraw Hill.,1968.

[20] A.G. Derneryd, "Linearly polarized microstrip antenna", *IEEE Trans. Antennas Propagat.*, pp.846-851, Nov., 1976.

[21] R.F. Harington, *Time Harmonic Electromagnetic Fields*", New York: McGraw Hill.,1961.

[22] E.O. Hammerstad,"Equations for Microstrip Design",*5th European Microwave Conf.*, pp.268-272, Sept.,1975.

[23] R.N. Ghose, *Microwave Circuit Theory and Design*, New York:McGraw Hill, 1963.

[24] R.E. Collin, *Foundations for Microwave Engineering*, New York: McGraw Hill, 1966.

[25] A.K. Bhattacharyya, *Generalized Transmission line model of Microstrip Antennas and Some Applications*, Ph.D. dissertation, IIT Kharagpur, India, 1985.

[26] K.R. Carver, "A modal expansion theory for microstrip antenna", *IEEE Int. Symp. Digest.* AP-S, Seattle, WA,pp. 101-104, June 1979.

[27] Y.T. Lo, D. Solomon, W.F. Richards, "Theory and experiment on microstrip antennas", *IEEE Trans. Antennas Propagat.*, vol.AP-27, pp.137-145, March 1979.

[28] Y.T. Lo, D. Solomon, F.R. Ore, D.D. Harrison and G.A, Deschamps,"Study of microstrip antennas, microstrip phased array, and microstrip feed network",*RADC*- TR-77-406, Dec.,1977.

[29] M. Ghaderi, *Investigations of Microstrip Periodic Structure*, M.Sc. dissertation, University of Saskatchewan, Canada, 1990.

[30] S. Ramo, J.R.Whinner, and T.V. Duzer, *Fields and Waves in Communication Electronics*, New York: John Wiley & Sons, 1967.

[31] N.C. Karmakar and A. Bhattacharyya, "Electromagnetically coupled microstrip patch antenna - theoretical and experimental investigations", *Microwave and Optical Technology Lett.*, College Station, Texas: John Wiley & Sons, No. 91193, (March-1992).

[32] W.A. Davis, *Microwave Circuit Theory and Analysis*, New York:McGraw Hill.,1984.

[33] *HP 8510 Network Analyzer System Operating and Programming Manual,* Hewlett-Packard Company, 1400 Fountaingrove Parkway, Santa Rosa, Ca 95401, U.S.A. Jan., 1985.

[34] *Operating and Programming Manual - HP 8510 Network Analyzer System,* Hewlett-Packard Company, 1400 Fountaingrove Parkway, Santa Rosa, Ca 95401, U.S.A. July, 1987.

APPENDIX: EXPERIMENTAL PROCEDURES

A.1 Introduction

To verify the theoretical methods undertaken in this thesis, the experimental data were collected by using the HP 8510B vector network analyzer. The HP 8510B network analyzer system is an advanced and sophisticated measurement instrument designed to make microwave measurements of any kinds [33]. But the basic principles to its operation are fairly simple. The system measures the magnitude and phase characteristics of networks and components such as filters, amplifiers, attenuators, and antennas. The information in this appendix provides with the basic measurement procedures of input impedance and return loss of an EMC patch antenna using the HP 8510B network analyzer.

A.2 Basic Network Measurements

With the network analyzer, two kinds of measurements are made: reflection measurements and transmission measurements [34]. An incident signal generated by an RF source controlled by the HP 8510B is applied to the test device and compared with the signal reflected from the device input or transmitted through it as shown in figure-A.1.

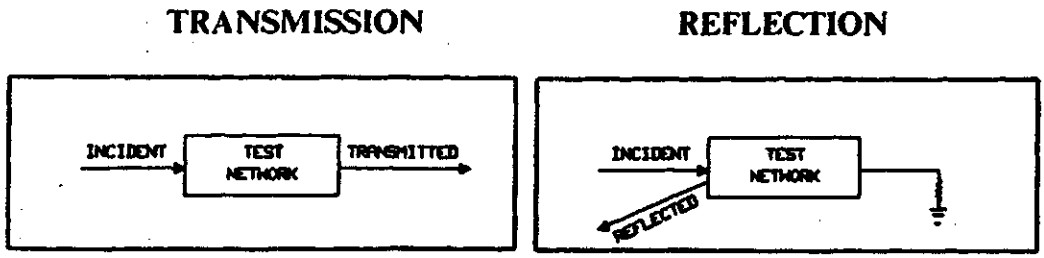

Figure-A.1 Transmission and reflection from a test network (from [33])

Reflection measurements are made by comparing the reflected signal to the incident signal. The results in measurement data on reflection characteristics of the device are in the following formats:

. Return loss,

. Standing Wave Ratio,

. Reflection Coefficient, and

. Impedance.

The return loss and input impedance measurements of the EMC patch antenna were used in this thesis.

a) Basic principle of the HP 8510B Network Analyzer

The HP 8510B network analyzer is a fully integrated vector network analyzer [34] which includes four essential parts:

. a source,

. a test set,

. a signal detector and analog-to-digital converter, and

. a digital microprocessor and display.

The source provides the RF signal. The test set separates this signal into an incident signal sent to the device-under-test and a reference signal against which the transmitted and reflected signals are later compared. It also receives transmitted and reflected signals from the device-under-test. The signal detector and analog-to-digital converter takes all of these signals and converts them to digital information for high-speed processing. The digital microprocessor controls the system, analyzes the digitized signals, correct errors, and display the results in a variety of formats.

In the HP 8510B network analyzer system, the essential parts are individual HP instruments together to make up the HP 8510 system. Shown in figure-A.2, it is a packaged as four major instruments [34]:

. HP 8510B Display/Processor

. HP 8510B IF detector

. HP 851X - series test set

. HP 834X - series synchronized sweeper or

. HP 835X - series sweep oscillator with an appropriate HP 835X-series plug-in.

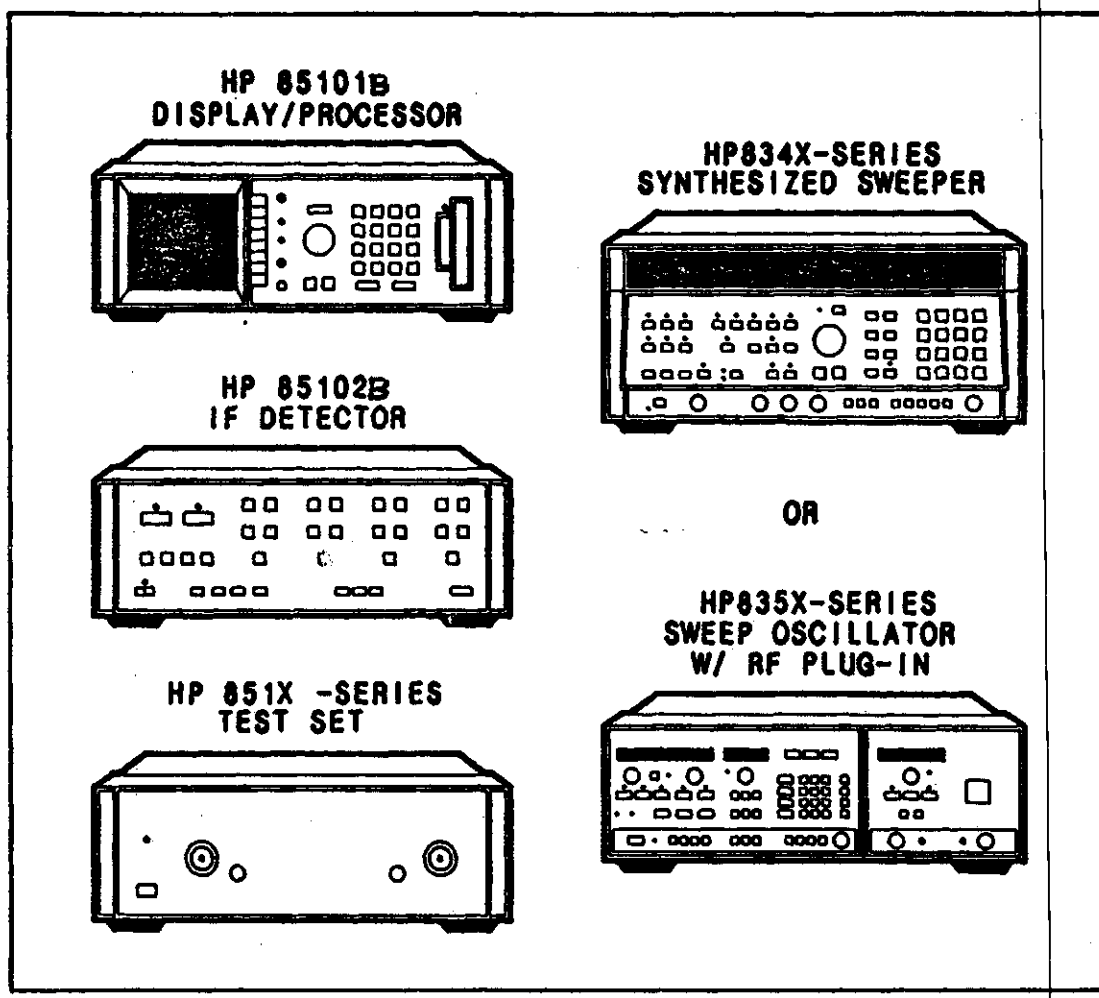

Figure-A.2 HP 8510 network analyzer system (from [33])

Additional system components can be included hardcopy output devices such as a printer and/or a plotter, and a disc unit. These peripheral

devices are controlled directly by the HP 8510 system. The data of the EMC patch antenna were taken from printer and plotter.

A.3 Experimental Setup and Data Collection

Figure-A.3 illustrates a complete experimental setup for the measurements of the input impedance and the return loss of an EMC patch antenna. The test device is the EMC patch antenna which is connected with the HP 851X test set via port#1. The CRT display was a Smith chart plot of the input impedance of the EMC patch antenna under test. The plotter and the line printer were collecting data into two different formats.

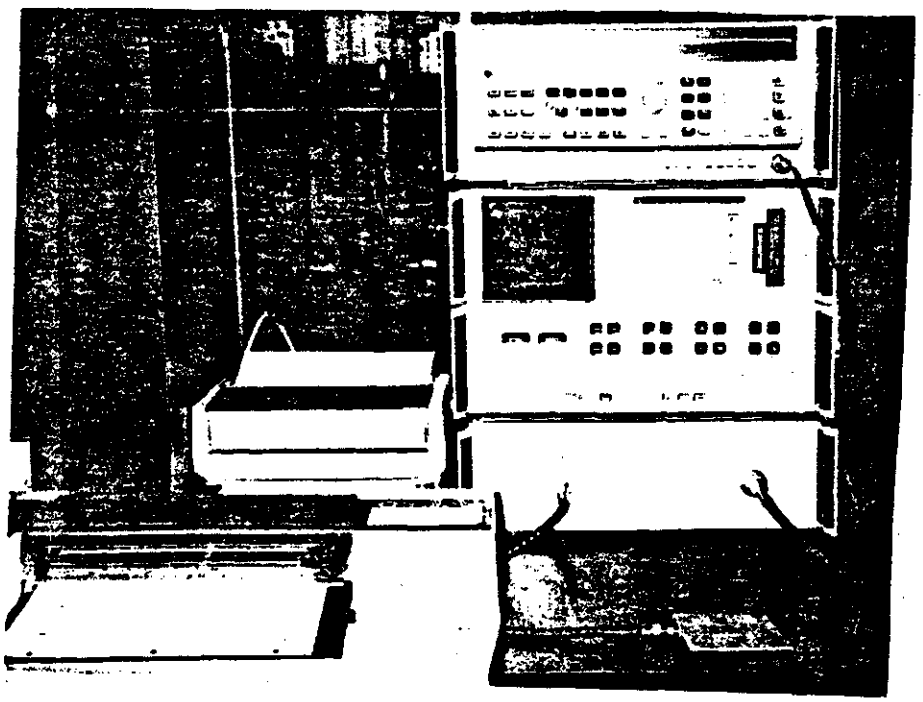

Figure-A.3 An experimental setup of the EMC patch antenna measurement using the HP 8510B network analyzer. The patch under test is shown in the bottom right portion of the picture

a) Input Impedance Data

Shown in figure-A.4 is a Smith chart plot normalized to a 50Ω input impedance obtained from the plotter for a patch of length 2.22cm, width 2.00cm and feed inset 1.11cm. The frequency range was selected from 3.75Ghz to 4.75Ghz. Marker 1 points at the input impedance reading of the EMC patch antenna at 4.27Ghz. The input impedance at 4.27Ghz was 84.344 + j18.332 ohms. The line printer output of the same is shown in the following page.

b) Return Loss Data

In figure-A.5 the return loss plot in log magnitude is shown for a patch of length 2.22cm, width 1.00cm at a feed inset 1.11cm. The frequency range used was from 4.00Ghz to 5.00Ghz. Marker 1 shows the return loss reading of the EMC patch antenna at 4.35Ghz. The return loss obtained was -11.051dB. The line printer output for the same is given in the following page.

Data for other patches and/or at different feed insets of the same patch were taken using the same measurement procedures.

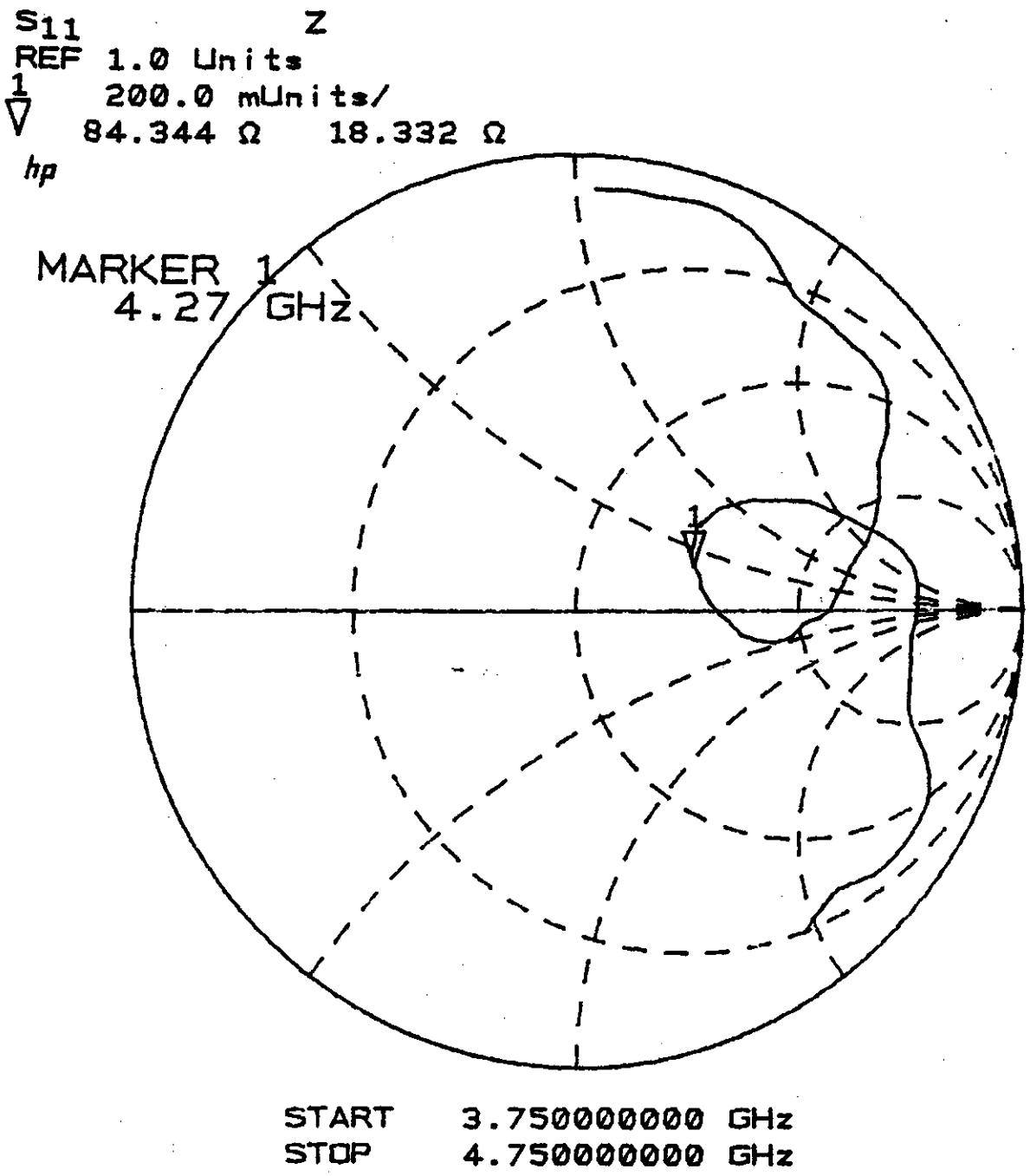

Figure-A.4 A Smith chart plot of the input impedance of an EMC patch antenna of length 2.22cm, width 2.00cm at a feed inset of 1.11cm obtained from the plotter by using the HP 8510B network Analyzer

Line printer output of the input impedance data of an EMC patch antenna of length 2.22cm, width 2.00cm at a feed inset of 1.11cm obtained by using the HP 8510B network Analyzer

No.	Freq. (Ghz)	R (Ohms)	X (Ohms)
0	3.750000000E+09	4.144531000E-00,	5.269530000E+01
1	3.760000000E+09	4.263671000E+00,	5.433397000E+01
2	3.770000000E+09	4.281250000E+00,	5.607031000E+01
3	3.780000000E+09	4.394531000E+00,	5.778515000E+01
4	3.790000000E+09	4.578124000E+00,	5.940820000E+01
5	3.800000000E+09	4.773437000E+00,	6.070898000E+01
6	3.810000000E+09	4.873046000E+00,	6.219140000E+01
7	3.820000000E+09	4.882812000E+00,	6.361132000E+01
8	3.830000000E+09	4.812499000E+00,	6.539843000E+01
9	3.840000000E+09	4.667968000E+00,	6.776562000E+01
10	3.850000000E+09	4.355468000E+00,	7.080858000E+01
11	3.860000000E+09	5.687499000E+00,	7.443359000E+01
12	3.870000000E+09	6.984375000E+00,	7.891639000E+01
13	3.880000000E+09	9.546874000E+00,	8.348827000E+01
14	3.890000000E+09	1.265937000E+01,	8.785154000E+01
15	3.900000000E+09	1.625000000E+01,	9.134373000E+01
16	3.910000000E+09	1.906250000E+01,	9.433671000E+01
17	3.920000000E+09	2.083593000E+01,	9.810938000E+01
18	3.930000000E+09	2.213672000E+01,	1.021914000E+02
19	3.940000000E+09	2.331640000E+01,	1.058594000E+02
20	3.950000000E+09	2.511718000E+01,	1.125508000E+02
21	3.960000000E+09	2.680859000E+01,	1.174336000E+02
22	3.970000000E+09	2.835156000E+01,	1.219633000E+02
23	3.980000000E+09	2.946875000E+01,	1.274648000E+02
24	3.990000000E+09	3.146875000E+01,	1.340078000E+02
25	4.000000000E+09	3.513281000E+01,	1.422812000E+02
26	4.010000000E+09	4.373437000E+01,	1.525156000E+02
27	4.020000000E+09	5.685936000E+01,	1.594531000E+02
28	4.030000000E+09	7.235713000E+01,	1.625078000E+02
29	4.040000000E+09	9.047655000E+01,	1.615391000E+02
30	4.050000000E+09	1.059922000E+02,	1.579687000E+02
31	4.060000000E+09	1.236875000E+02,	1.571172000E+02
32	4.070000000E+09	1.473359000E+02,	1.517890000E+02
33	4.080000000E+09	1.761172000E+02,	1.349756000E+02
34	4.090000000E+09	1.926953000E+02,	1.053594000E+02
35	4.100000000E+09	1.946562000E+02,	7.589061000E+01
36	4.110000000E+09	1.948984000E+02,	5.742968000E+01
37	4.120000000E+09	1.938594000E+02,	4.030468000E+01
38	4.130000000E+09	1.895547000E+02,	2.319531000E+01
39	4.140000000E+09	1.834687000E+02,	0.500781000E+01
40	4.150000000E+09	1.724297000E+02,	-0.500000000E+01
41	4.160000000E+09	1.579375000E+02,	-0.958594000E+01
42	4.170000000E+09	1.548359000E+02,	-1.053125000E+01
.	.	.	.
.	.	.	.

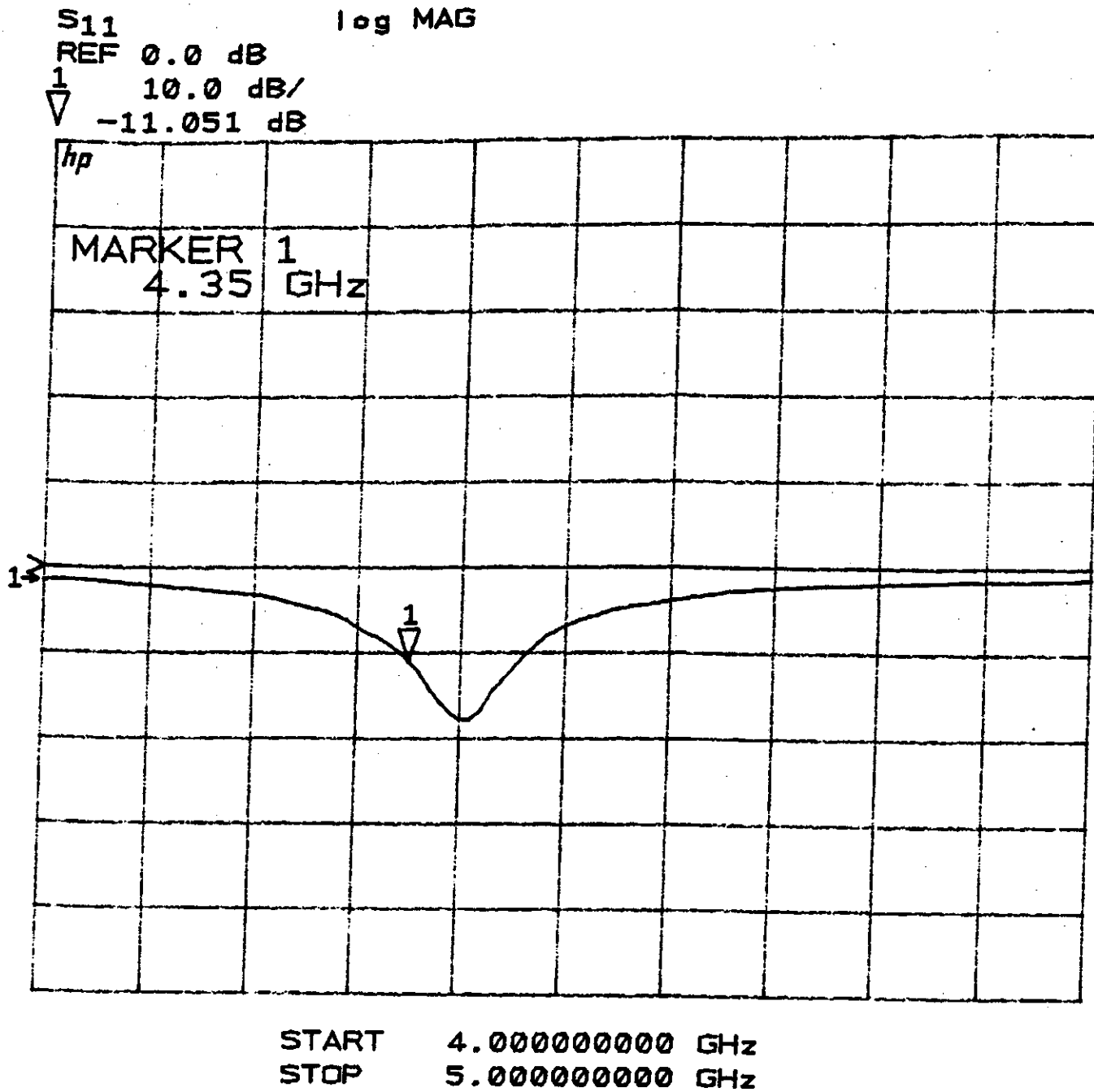

Figure-A.5 A log magnitude plot of the return loss of an EMC patch antenna of length 2.22cm, width 2.00cm at a feed inset of 1.11cm obtained from the plotter by using the HP 8510B network Analyzer

Line printer output of the return loss of an EMC patch antenna of length 2.22cm, width 2.00cm at a feed inset of 1.11cm obtained by using the HP 8510B network Analyzer

No.	Freq. (Ghz)	RL (-dB)	
0	4.000000000000E+09	-1.525330000000E+00,	0.000000000000E+00
1	4.010000000000E+09	-1.456804000000E+00,	0.000000000000E+00
2	4.020000000000E+09	-1.412292000000E+00,	0.000000000000E+00
3	4.030000000000E+09	-1.461731000000E+00,	0.000000000000E+00
4	4.040000000000E+09	-1.539917000000E+00,	0.000000000000E+00
5	4.050000000000E+09	-1.681396000000E+00,	0.000000000000E+00
6	4.060000000000E+09	-1.776550000000E+00,	0.000000000000E+00
7	4.070000000000E+09	-1.868042000000E+00,	0.000000000000E+00
8	4.080000000000E+09	-1.967102000000E+00,	0.000000000000E+00
9	4.090000000000E+09	-2.055542000000E+00,	0.000000000000E+00
10	4.100000000000E+09	-2.144165000000E+00,	0.000000000000E+00
11	4.110000000000E+09	-2.239368000000E+00,	0.000000000000E+00
12	4.120000000000E+09	-2.343750000000E+00,	0.000000000000E+00
13	4.130000000000E+09	-2.437744000000E+00,	0.000000000000E+00
14	4.140000000000E+09	-2.518066000000E+00,	0.000000000000E+00
15	4.150000000000E+09	-2.605469000000E+00,	0.000000000000E+00
16	4.160000000000E+09	-2.733887000000E+00,	0.000000000000E+00
17	4.170000000000E+09	-2.840332000000E+00,	0.000000000000E+00
18	4.180000000000E+09	-2.882556000000E+00,	0.000000000000E+00
19	4.190000000000E+09	-3.035522000000E+00,	0.000000000000E+00
20	4.200000000000E+09	-3.135376000000E+00,	0.000000000000E+00
21	4.210000000000E+09	-3.262329000000E+00,	0.000000000000E+00
22	4.220000000000E+09	-3.515503000000E+00,	0.000000000000E+00
23	4.230000000000E+09	-3.847168000000E+00,	0.000000000000E+00
24	4.240000000000E+09	-4.237061000000E+00,	0.000000000000E+00
25	4.250000000000E+09	-4.583252000000E+00,	0.000000000000E+00
26	4.260000000000E+09	-4.944238000000E+00,	0.000000000000E+00
27	4.270000000000E+09	-5.141113000000E+00,	0.000000000000E+00
28	4.280000000000E+09	-5.515723000000E+00,	0.000000000000E+00
29	4.290000000000E+09	-6.261475000000E+00,	0.000000000000E+00
30	4.300000000000E+09	-7.071533000000E+00,	0.000000000000E+00
31	4.310000000000E+09	-7.817871000000E+00,	0.000000000000E+00
32	4.320000000000E+09	-9.255859000000E+00,	0.000000000000E+00
33	4.330000000000E+09	-8.958008000000E+00,	0.000000000000E+00
34	4.340000000000E+09	-9.802246000000E+00,	0.000000000000E+00
35	4.350000000000E+09	-1.099976000000E+01,	0.000000000000E+00
36	4.360000000000E+09	-1.220898000000E+01,	0.000000000000E+00
37	4.370000000000E+09	-1.410400000000E+01,	0.000000000000E+00
38	4.380000000000E+09	-1.578662000000E+01,	0.000000000000E+00
39	4.390000000000E+09	-1.668579000000E+01,	0.000000000000E+00
40	4.400000000000E+09	-1.836426000000E+01,	0.000000000000E+00
41	4.410000000000E+09	-1.827988000000E+01,	0.000000000000E+00
42	4.420000000000E+09	-1.754395000000E+01,	0.000000000000E+00
.	.	.	.
.	.	.	.
.	.	.	.